Rhenium carbonyl complexes bearing methylated triphenylphosphonium cations as antibody-free mitochondria trackers for X-ray fluorescence imaging

Gabrielle Schanne,[a] Lucas Henry,[a] How Chee Ong,[b] Andrea Somogyi,[c] Kadda Medjoubi,[c] Nicolas Delsuc,[a] Clotilde Policar,[a] Felipe García,[b*] Helene C. Bertrand[a,b*]

[a] Laboratoire des biomolécules, LBM, Département de chimie, Ecole normale supérieure, PSL University, Sorbonne université, CNRS, 75005 Paris, France.
E-mail: helene.bertrand@ens.psl.eu
[b] School of Physical and Mathematical Sciences, Division of Chemistry and Biological Chemistry, Nanyang Technological University, 21 Nanyang Link, 637371, Singapore
E-mail: fgarcia@ntu.edu.sg
[c] Synchrotron SOLEIL, BP 48, Saint-Aubin, 91192 Gif sur Yvette, France

Supporting Information

Experimental part

Synthesis

General considerations

^{1}H and ^{13}C NMR spectra were recorded on a Bruker DRX 300 using solvent residuals as internal references. The following abbreviations are used: singlet (s), doublet (d), doubled doublet (dd), triplet (t), doubled triplet (td), quadruplet (q) and multiplet (m). High resolution mass spectrometry (HRMS) was performed on a Bruker hybride APEX spectrometer (electrospray) at the ICMMO (Institut de chimie et des matériaux d'Orsay). The following abbreviations are used: electrospray (ESI), time of flight (TOF). TLC analysis was carried out on silica gel (Merck 60F-254) with visualization at 254 and 366 nm. Preparative flash chromatography was carried out with Merck silica gel (Si 60, 40-63 µm). Reagents and chemicals were purchased from Merck, Acros, Alfa Aesar, TCI or Strem Chemicals. Dry solvents (dichloromethane (CH_2Cl_2 or DCM), toluene, tetrahydrofuran (THF) and dimethylformamide (DMF)) and reagents (diisopropylethylamine (DIEA)) were purchased from Merck and used without further purification. Analytical HPLC was performed on an Agilent 1200 series equipped with a quaternary pump using a Proto 200 C18 from Higgins Analytical Inc (particles size 3 µm, 100 × 4.6 mm column). Preparative HLC was performed on an Agilent 1260 Infinity using a Nucleodur C18 HTech column from Macherey-Nagel Inc. (particles size 5 µm, 250 × 16 mm column). UV-visible absorption spectra were recorded on a Varian Cary 300 Bio spectrophotometer, luminescence emission spectra on a Jasco FP-8300 spectrofluorimeter. Infrared spectra were recorded on a Perkin Elmer Spectrum 100 in ATR mode (background on air) and analyzed using the Omnic software. The following abbreviations are used: weak (w), strong (S), broad (br). TP*P (2-aminoethyl)triphenylphosphonium bromide derivatives were synthesized according to published procedures.[1]
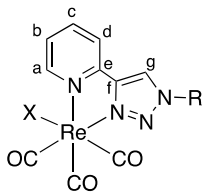
Numbering used in the NMR attributions.

β-Alanine(*N*-2-chloroacetyl) *tert*-butyl ester 1: β-alanine tert-butyl ester hydrochloride (1.50 g, 8.26 mmol, 1.2 eq.) was suspended in dry DCM (15 mL) under argon. Dry DIEA (2.9 mL, 17.2 mmol, 2.5 eq.) was added and the suspension was cooled down in an ice bath. Chloroacetyl chloride (0.6 mL, 6.9 mmol, 1.0 eq.) was added dropwise and the reaction mixture was stirred for 1 h at room temperature (ca. 25 °C). The reaction mixture was then diluted with DCM (15 mL) and washed with a 0.1 M HCl aqueous solution (30 mL), a 10 % $NaHCO_3$ aqueous solution (30 mL) and brine (30 mL). The organic phase was dried over $MgSO_4$, filtered and evaporated to afford β-alanine(*N*-2-chloroacetyl) *tert*-butyl ester **1** as a pale-yellow oil (1.61 g, quantitative yield).

Rf(SiO_2, cyclohexane/ethyl acetate 70:30 v:v) = 0.28); ^1H NMR (300 MHz, $CDCl_3$): δ (ppm) 7.16 (broad s, 1H, N*H*), 3.92 (s, 2H, Cl-C*H$_2$*), 3.41 (q, 2H, *J* = 6.1 Hz, CONH-C*H$_2$*), 2.36 (t, 2H, *J* = 6.1 Hz, C*H$_2$*-COOtBu), 1.34 (s, 9H, -C(C*H$_3$*)$_3$); ^{13}C NMR (75 MHz, $CDCl_3$): δ (ppm) 172.1 (*C*OOtBu), 165.8 (*C*ONH), 81.1 (-*C*(CH$_3$)$_3$), 42.5 (Cl-*C*H$_2$), 35.3 (NH-*C*H$_2$), 34.8 (NH-CH$_2$-*C*H$_2$), 27.9 (-C(*C*H$_3$)$_3$); HRMS (ESI+): m/z calculated for $C_9H_{16}ClNNaO_3$ [M + Na]$^+$: 244.0711, found: 244.0722.

***tert*-Butyl 3-(2-azidoacetamido)propanoate 2:** β-alanine(*N*-2-chloroacetyl)*tert*-butyl ester **1** (1.02 g, 4.58 mmol, 1.0 eq.) was dissolved in a 3:1 v:v mixture of acetone (15 mL) and water (5 mL). NaN_3 (587.1 mg, 9.16 mmol, 1.97 eq.) and NaI (69.1 mg, 461 µmol, 0.1 eq.) were added and the reaction mixture was stirred for 17 h at 50 °C. NaI (0.1 eq.) was added again and the reaction stirred for one additional hour. Acetone was evaporated and the mixture was diluted with DCM (15 mL) and water (5 mL). The aqueous phase was extracted with DCM (3 × 10 mL); the combined organic phases were dried over $MgSO_4$, filtered and evaporated to afford *tert*-butyl 3-(2-azidoacetamido)propanoate **2** as a pale-yellow oil (0.93 g, 89% yield).

Rf(SiO_2, cyclohexane/ethyl acetate 70:30 v:v) = 0.22); ^1H NMR (300 MHz, $CDCl_3$): δ (ppm) 7.00 (broad s, 1H, N*H*), 3.79 (s, 2H, N$_3$-C*H$_2$*), 3.35 (q, 2H, *J* = 6.2 Hz, NH-C*H$_2$*), 2.32 (t, 2H, *J* = 6.2 Hz, NH-CH$_2$-C*H$_2$*), 1.30 (s, 9H, -C(C*H$_3$*)$_3$); ^{13}C NMR (75 MHz, $CDCl_3$): δ (ppm) 171.1 (*C*OOtBu), 166.6 (*C*ONH), 80.9 (-*C*(CH$_3$)$_3$), 52.2 (N$_3$-*C*H$_2$), 34.8 (NH-*C*H$_2$), 34.7 (NH-CH$_2$-*C*H$_2$), 27.7 (-C(*C*H$_3$)$_3$); IR: 3304 (br, NH), 2980 (w, CH), 2102 (S, N$_3$), 1723, 1659 (S, C−O). HRMS (ESI+): m/z calculated for $C_9H_{16}N_4NaO_3$ [M + Na]$^+$: 251.1115, found: 251.1118.

***tert*-Butyl 3-(2-(4-(pyridin-2-yl)-1*H*-1,2,3-triazol-1-yl)acetamido)propanoate 3:** *tert*-butyl 3-(2-azidoacetamido)propanoate **2** (485.0 mg, 2.12 mmol, 1.0 eq.) was dissolved in a 2:1 v:v mixture of acetone (20 mL) and water (10 mL). 2-Ethynylpyridine (264.0 mg, 2.56 mmol, 1.2 eq.), copper sulfate pentahydrate (87.7 mg, 549 µmol, 0.26 eq.) and sodium ascorbate (434 mg, 2.19 mmol, 1.03 eq.) were then added and the suspension was sonicated for a few minutes, during which a light brownish precipitate formed. The reaction mixture was then stirred for 2 h at room temperature (ca. 25 °C). Acetone was evaporated, the mixture was diluted with DCM (30 mL), and the resulting solution was poured into an aqueous 28 % ammonia solution (30 mL) and extracted

with DCM (3 × 10 mL). The organic phases were combined, dried over Na_2SO_4, filtered and concentrated. The resulting brown solid was purified by column chromatography on silica gel (ethyl acetate/cyclohexane 60:40 to 100:0 v:v) to afford *tert*-butyl 3-(2-(4-(pyridin-2-yl)-1*H*-1,2,3-triazol-1-yl)acetamido)propanoate **3** as a white solid (598.4 mg, 85% yield).

Rf(SiO_2, ethyl acetate) = 0.23); ^1H NMR (300 MHz, $CDCl_3$): δ (ppm) 8.59 (d, 1H, *J* = 5.0 Hz, H^a pyta), 8.37 (s, 1H, H^g pyta), 8.19 (d, 1H, *J* = 7.9 Hz, H^d pyta), 7.82 (td, 1H, *J* = 7.9, 1.8 Hz, H^c pyta), 7.33-7.27 (m, 1H, H^b pyta), 6.60 (broad s, 1H, N*H*), 5.11 (s, 2H, pyta-C*H$_2$*), 3.50 (q, 2H, *J* = 6.2 Hz, CONH-C*H$_2$*), 2.43 (t, 2H, *J* = 6.2 Hz, C*H$_2$*-COOtBu), 1.38 (s, 9H, -C-(C*H$_3$*)$_3$); ^{13}C NMR (75 MHz, $CDCl_3$): δ (ppm) 171.5 (*C*OOtBu), 164.9 (*C*ONH), 149.4 (C^e pyta), 148.9 (C^a pyta), 148.3 (C^f pyta), 137.8 (C^c pyta), 124.1 (C^g pyta), 123.4 (C^b pyta), 120.7 (C^d pyta), 81.6 (-*C*(CH$_3$)$_3$), 53.3 (pyta-*C*H$_2$), 35.5 (NH-*C*H$_2$), 34.9 (NH-CH$_2$-*C*H$_2$), 28.1 (-C(*C*H$_3$)$_3$); IR: 3357 (S, CH aromatic), 2985 (w, CH aliphatic), 1712, 1681 (S, C−O); HRMS (ESI+): m/z calculated for $C_{16}H_{21}N_5NaO_3$ [M + Na]$^+$: 354.1537, found: 354.1529.

Re(CO)$_3$Cl(*tert*-butyl 3-(2-(4-(pyridin-2-yl)-1*H*-1,2,3-triazol-1-yl)acetamido)propanoate) 4: *tert*-butyl 3-(2-(4-(pyridin-2-yl)-1*H*-1,2,3-triazol-1-yl)acetamido)propanoate **3** (399.8 mg, 1.21 mmol, 1.0 eq.) was dissolved in hot toluene (60 °C, 20 mL), Re(CO)$_5$Cl (484.1 mg, 1.34 mmol, 1.1 eq.) was added and the reaction mixture was refluxed for 5 h. The reaction mixture was cooled down to room temperature, the precipitated solid was filtered, washed with cold toluene (0 °C, 10 mL) and dried under vacuum to afford Re(CO)$_3$Cl(*tert*-butyl 3-(2-(4-(pyridin-2-yl)-1*H*-1,2,3-triazol-1-yl)acetamido)propanoate) **4** as a yellow solid (880.0 mg, 99% yield).

Rf(SiO_2, ethyl acetate) = 0.34; ^1H NMR (300 MHz, $CDCl_3$): δ (ppm) 9.02 (ddd, 1H, *J* = 5.6, 1.5, 0.8 Hz, H^a pyta), 8.54 (s, 1H, H^g pyta), 8.06 (td, 1H, *J* =7.8, 1.5 Hz, H^c pyta), 7.91 (dt, *J* = 7.8, 1.2 Hz, 1H, H^d pyta), 7.47 (ddd, 1H, *J* = 7.8, 5.6, 1.2 Hz, H^b pyta), 7.19 (t, 1H, *J* = 5.8 Hz, N*H*), 5.22-4.89 (m, 2H, pyta-C*H$_2$*), 3.52 (qd, 2H, *J* = 6.6, 2.2 Hz, NH-C*H$_2$*), 2.48 (t, 2H, *J* = 6.6 Hz, C*H$_2$*-COOtBu), 1.46 (s, 9H, -C(C*H$_3$*)$_3$); ^{13}C NMR (75 MHz, CD_3OD): δ (ppm) 172.6 (*C*OOtBu), 166.5 (*C*ONH), 154.3 (C^f pyta), 150.8 (C^e pyta), 150.2 (C^a pyta), 141.4 (C^c pyta), 127.9 (C^g pyta), 127.3 (C^b pyta), 123.6 (C^d pyta), 82.1 (-*C*(CH$_3$)$_3$), 54.3 (pyta-*C*H$_2$), 36.9 (NH-*C*H$_2$), 35.9 (NH-CH$_2$-*C*H$_2$), 28.4 (-C(*C*H$_3$)$_3$); IR: 3288 (br, NH), 2980 (w, CH), 2021 (s, CO A$_1$), 1883 (s, CO E), 1681 (s, C=O), 1153 (S, C-O); HRMS (ESI+): m/z calculated for $C_{19}H_{21}ClN_5NaO_6Re$ [M + Na]$^+$: 635.9657, found: 635.9355.

Re(CO)$_3$Cl(3-(2-(4-(pyridin-2-yl)-1*H*-1,2,3-triazol-1-yl)acetamido)propanoic acid) 5: Re(CO)$_3$Cl(*tert*-butyl 3-(2-(4-(pyridin-2-yl)-1*H*-1,2,3-triazol-1-yl)acetamido)propanoate) **4** (880.0 mg, 1.38 mmol, 1 eq.) was dissolved in DCM (4 mL) and trifluoroacetic acid (4 mL, 52 mmol, 35 eq.) was added slowly. The reaction mixture was stirred at room temperature for 1 h. The solvents were evaporated and concentrated HCl (37%, 4 mL) was added. The reaction mixture was stirred for 10 min at room temperature, HCl was evaporated and the residue dried under vacuum to afford Re(CO)$_3$Cl(3-(2-(4-(pyridin-2-yl)-1*H*-1,2,3-triazol-1-yl)acetamido)propanoic acid) **5** as a whitish solid (650.0 mg, 86% yield).

Rf(SiO_2, DCM/EtOH 75:25 v:v + 1% v CH$_3$COOH) = 0.61; ^1H NMR (300 MHz, $CDCl_3$/CD_3OD): δ (ppm) 8.97 (dt, 1H, *J* = 5.5, 1.2 Hz, H^a pyta), 8.93 (s, 1H, H^g pyta), 8.18-8.08 (m, 2H, Hc & H^d pyta), 7.54 (td, 1H, *J* = 5.5, 4.0 Hz, H^b pyta), 5.45-5.25 (m, 2H, pyta-C*H$_2$*), 3.52 (t, 2H, *J* = 6.6 Hz, NH-C*H$_2$*), 2.57 (t, 2H, *J* = 6.6 Hz, C*H$_2$*-COOH); ^{13}C NMR (75 MHz, $CDCl_3$/CD_3OD): δ (ppm) 173.6 (*C*OOH), 164.4

(*C*ONH), 152.7 (C^f pyta), 149.1 (C^e pyta), 148.6 (C^a pyta), 139.6 (C^c pyta), 128.5 (C^g pyta), 127.7 (C^b pyta), 125.6 (C^d pyta), 122.0, 52.8 (pyta-*C*H$_2$), 35.4 (NH-*C*H$_2$), 33.0 (NH-CH$_2$-*C*H$_2$); IR: 3353, (br, OH), 3129 (w, CH), 2015 (s, CO A$_1$), 1897.6 (s, CO E), 1719 (s, C=O); HRMS (ESI+): m/z calculated for C$_{15}$H$_{13}$ClN$_5$NaO$_6$Re [M + Na]$^+$: 603.9995, found: 603.9991.

(2-Aminoethyl)triphenylphosphonium bromide:[1] (2-bromoethyl) amine hydrobromide (7.81 g, 38.1 mmol, 1.0 eq.) was dissolved in acetonitrile (50 mL). Triphenylphosphine (10.0 g, 38.1 mmol, 1.0 eq.) was added and the solution was refluxed overnight (82 °C). The precipitate was filtered, dissolved in water and treated with a saturated aqueous solution of K$_2$CO$_3$ until pH > 11. The product was extracted with DCM (3 × 10mL); the organic phases were combined, dried over MgSO$_4$ and evaporated to afford (2-aminoethyl)triphenylphosphonium bromide as a white solid (4.47 g, 30% yield).
Rf(SiO$_2$, DCM/EtOH 70:30 v:v) = 0.39 ; ^{1}H NMR (300 MHz, CDCl$_3$): δ (ppm) 7.75 (m, 15 H, PPh$_3$), 4.06 (m, 2H, *J* = 1.1 Hz, H$_2$N-C*H$_2$*), 3.15 (m, 2H, *J* = 1.1 Hz, C*H$_2$*-PPh$_3$); IR: 3316 (w, NH), 2903 (w, CH), 1743 (C=C); HRMS (ESI+): m/z calculated for [C$_{20}$H$_{21}$NP]$^+$: 306.139502, found: 306.140613. NMR Data in agreement with literature.

(2-ammonioethyl)tri(p-tolyl)phosphonium bromide: (2-bromoethyl) amine hydrobromide (0.410 g, 2 mmol, 1.0 eq.) was dissolved in acetonitrile (5 mL). Tri(p-tolyl)phosphine (0.898 g, 2.95 mmol, 1.475 eq.) was added and the solution was refluxed overnight (82 °C). The solution was allowed to cool to room temperature and the product was precipitated by the addition of diethyl ether. The solid was filtered and recrystallized in ACN/Et$_2$O to afford (2-ammonioethyl)tri(p-tolyl)phosphonium bromide as a white solid (0.405 g, 40% yield).
^{1}H NMR (500 MHz, CDCl$_3$): δ (ppm) 8.94 (s, 3 H, -N*H$_3$*), 7.73 – 7.36 (m, 12 H, Ar-*H*), 4.35 (m, 2 H, H$_3$N-C*H$_2$*), 3.33 (s, 2 H, C*H$_2$*-PAr$_3$), 2.51 (s, 9 H, Ar-*Me*); ^{31}P{^{1}H} NMR (121 MHz, CDCl$_3$): δ (ppm) 21.58.

(2-ammonioethyl)tris(3,5-dimethylphenyl)phosphonium bromide: (2-bromoethyl) amine hydrobromide (0.246 g, 1.2 mmol, 1.0 eq.) was dissolved in acetonitrile (3 mL). Tris(3,5-dimethylphenyl)phosphine (0.555 g, 1.60 mmol, 1.33 eq.) was added and the solution was refluxed overnight (82 °C). The solution was allowed to cool to room temperature and the product was precipitated by the addition of diethyl ether. The solid was filtered and recrystallized in ACN/Et$_2$O to afford (2-ammonioethyl)tris(3,5-dimethylphenyl)phosphonium bromide as a white solid (0.425 g, 64% yield).[1]
^{1}H NMR (500 MHz, CDCl$_3$): δ (ppm) 8.76 (s, 3 H, -N*H$_3$*), 7.42 (s, 3 H, o-Ph), 7.31 (d, J$_{P-H}$ = 14.1 Hz, 6 H), 4.39 – 4.17 (m, 2 H, H$_2$N-C*H$_2$*), 3.31 (s, 2 H, C*H$_2$*-PAr$_3$), 2.43 (s, 18 H, Ar-*Me*); ^{31}P{^{1}H} NMR (121 MHz, CDCl$_3$): δ (ppm) 21.34.

General procedure for conjugates 1-3:

Re(CO)$_3$Cl(3-(2-(4-(pyridin-2-yl)-1*H*-1,2,3-triazol-1-yl)acetamido)propanoic acid) **5** (1.0 eq.), N-ethyl-N'-(3-dimethylaminopropyl)carbodiimide hydrochloride (EDC·HCl, 1.5 eq.) and hydroxybenzotriazole (HOBt, 1.5 eq.) were dissolved in DMF (2.8 mL / 100 mg). After 5 min of stirring, (2-aminoethyl)triphenylphosphonium bromide derivative **P1-3** (1.1 eq.) and DIEA (3.3 eq.) were added and the reaction mixture was stirred at room temperature (ca. 25 °C) for 24 or

48 h. After evaporation of the solvent, the resulting solid was dissolved in DCM (15 mL) and a saturated aqueous $NaHCO_3$ solution (15 mL) was added. The aqueous phase was extracted with DCM (10 mL); the combined organic phases were dried over Na_2SO_4, filtered and evaporated. The crude product was purified by column chromatography on aluminum oxide with a DCM/EtOH gradient from 100:0 to 80:20 v:v as eluent.

[Re(CO)$_3$Cl(triphenyl(2-(3-(2-(4-(pyridin-2-yl)-1H-1,2,3-triazol-1-yl)acetamido)propanamido)ethyl)phosphonium bromide)] C1: was obtained following general procedure from Re(CO)$_3$Cl(3-(2-(4-(pyridin-2-yl)-1*H*-1,2,3-triazol-1-yl)acetamido)propanoic acid) **5** (100.7 mg, 173.3 µmol, 1.0 eq.) and (2-aminoethyl)triphenylphosphonium bromide **P1** (90.3 mg, 193 µmol, 1.1 eq.) in 48 h after purification by column chromatography on aluminum oxide, DCM/EtOH gradient from 100:0 to 80:20 v:v: as a yellow sticky solid (74.7 mg, 70 % yield).

^{1}H NMR (300 MHz, CDCl$_3$): δ (ppm) 9.23 (s, 1H, H^g pyta), 8.99 (t, 1H, J = 5.4 Hz, N*H*), 8.88 (dd, 1H, J = 5.6, 1.3 Hz, H^a pyta), 8.56 (t, 1H, J = 5.1, N*H*), 8.03 (d, 1H, J = 7.6 Hz, H^d pyta), 7.94 (td, 1H, J = 7.6, 1.3 Hz, H^c pyta), 7.82-7.73 (m, 9H, PPh$_3$), 7.67 (m, 6H, PPh$_3$), 7.34 (dd, J = 7.6, 5.6 Hz, 1H, H^b pyta), 5.45 (s, 2H, pyta-C*H$_2$*), 3.80 (m, 2H, CONH-C*H$_2$*), 3.59-3.40 (m, 4H, 2 × C*H$_2$*), 2.32 (t, 2H, J = 5.7 Hz, C*H$_2$*); ^{13}C NMR (75 MHz, CDCl$_3$): δ (ppm) 172.5 (*C*ONH), 164.7 (*C*ONH), 152.8 (C^a pyta), 149.6 (C^f pyta), 148.7 (C^e pyta), 139.9 (C^c pyta), 135.5 (PPh$_3$ C$_{para}$), 135.4 (C^b pyta), 133.8, 133.7 (PPh$_3$ C$_{ortho}$), 130.8, 130.6 (PPh$_3$ C$_{meta}$), 125.7 (C^d pyta), 122.9 (C^g pyta), 118.6, 117.4 (Ph$_3$P-*C*), 60.3 (pyta-*C*H$_2$), 36.8 (NH-*C*H$_2$), 36.3 (NH-*C*H$_2$), 27.6 (NH-CH$_2$-*C*H$_2$); ^{31}P NMR (121 MHz, CDCl$_3$): δ (ppm) 21.06; IR: 3207 (br, NH), 3059 (w, CH aromatic), 2927 (w, CH aliphatic), 2020 (S, CO A$_1$), 1911 (S, CO E), 1885 (S, CO E), 1684 (C=O amide); HRMS (ESI+): m/z calculated for [C$_{35}$H$_{32}$ClN$_6$O$_5$PRe]$^+$: 869.1413 found: 869.1390; HPLC (5 to 100 % of acetonitrile in 10 min): t$_r$ = 6.4 min, purity > 85%.

[Re(CO)$_3$Cl((2-(3-(2-(4-(pyridin-2-yl)-1*H*-1,2,3-triazol-1-yl)acetamido)propanamido)ethyl)tri-*p*-tolylphosphonium bromide)] C2: was obtained following general procedure from Re(CO)$_3$Cl(3-(2-(4-(pyridin-2-yl)-1*H*-1,2,3-triazol-1-yl)acetamido)propanoic acid) **5** (100.1 mg, 172 µmol, 1.1 eq) and (2-aminoethyl)tri-p-tolylphosphonium bromide **P2** (79.1 mg, 155 µmol, 1.0 eq.) in 24 h after purification by column chromatography on aluminum oxide, DCM/EtOH gradient from 100:0 to 80:20 v:v: as a yellow solid (30.0 mg, 20 % yield).

^{1}H NMR (300 MHz, CDCl$_3$): δ (ppm) 9.20 (s, 1H, H^g pyta), 8.94-8.87 (m, 2H, H^a pyta & N*H*), 8.53 (t, 1H, J = 5.6 Hz, N*H*), 8.03 (m, 1H, H^d pyta), 7.94 (td, 1H, J = 7.6, 1.5 Hz, H^c pyta), 7.64-7.55 (m, 6H, PPh$_3$), 7.45 (dd, 6H, J = 8.2, 3.3 Hz, 6H, PPh$_3$), 7.34 (ddd, 1H, J = 7.6, 5.5, 1.5 Hz, H^b pyta), 5.43 (s, 2H, pyta-C*H$_2$*), 3.69-3.56 (m, 2H, CONH-C*H$_2$*), 3.50 (m, 2 × C*H$_2$*), 2.45 (s, 9H, 3 × C*H$_3$*), 2.36 (t, 2H, J = 5.9 Hz, 2H, C*H$_2$*); ^{13}C NMR (75 MHz, CDCl$_3$): δ (ppm) 172.4 (*C*ONH), 164.6 (*C*ONH), 149.6 (C^f pyta), 148.7 (C^e pyta), 146.7, 146.6 (PPh$_3$ C$_{para}$), 139.5 (C^a pyta), 133.6, 133.5 (PPh$_3$ C$_{ortho}$), 133.5 (C^c pyta), 131.4, 131.2 (PPh$_3$ C$_{meta}$), 125.7 (C^b pyta), 123.2 (C^d pyta), 122.7 (C^g pyta), 115.3, 114.2 (PPh$_3$-*C*), 54.0 (pyta-*C*H$_2$), 33.7 (NH-CH$_2$-*C*H$_2$); ^{31}P NMR (121 MHz, CDCl$_3$): δ (ppm) 19.94; IR: 3225 (br, NH), 3048 (w, CH aromatic), 2924 (w, CH aliphatic), 2020 (S, CO A$_1$), 1910 (S, CO E), 1882 (S, CO E), 1665 (C=O amide); HRMS (ESI+): m/z calculated for [C$_{38}$H$_{38}$ClN$_6$O$_5$PRe]$^+$: 911.1875 found: 911.1858; HPLC (5 to 100 % of acetonitrile in 10 min): t$_r$ = 7.93 min, purity > 85 %.

[Re(CO)₃Cl(tris(3,5-dimethylphenyl)(2-(3-(2-(4-(pyridin-2-yl)-1H-1,2,3-triazol-1-yl)acetamido)propanamido)ethyl)phosphonium bromide)] C3: was obtained following general procedure from Re(CO)₃Cl(3-(2-(4-(pyridin-2-yl)-1*H*-1,2,3-triazol-1-yl)acetamido)propanoic acid) **5** (99.8 mg, 172 µmol, 1.1 eq) and (2-aminoethyl)tris(3,5-dimethylphenyl)phosphonium bromide **P3** (85.8 mg, 156 µmol, 1.0 eq.) in 24 h after purification by column chromatography on aluminium oxide, DCM/EtOH gradient from 100:0 to 80:20 v:v: as a yellow sticky solid (62.9 mg, 39 %yield).

^{1}H NMR (300 MHz, CDCl₃): δ (ppm) 9.18 (s, 1H, H^g pyta), 9.14 (t, 1H, *J* = 5.4 Hz, N*H*), 8.92-8.89 (dt, 1H, *J* = 5.4, 1.2 Hz, H^a pyta), 8.56 (m, 1H, N*H*), 7.95-7.93 (m, 2H, H$^{d\&c}$ pyta), 7.37 (s, 3H, PPh₃), 7.36-7.32 (m, 4H, H^b pyta + PPh₃), 7.27 (s, 3H, PPh₃), 5.40 (m, 2H, C*H*₂), 5.29 (s, 2H, pyta-C*H*₂), 3.59-3.46 (m, 6H, 3 x C*H*₂), 2.40 (s, 18H, 6 x C*H*₃); ^{13}C NMR (75 MHz, CDCl₃): δ (ppm) 172.3 (*C*ONH), 164.5 (*C*ONH), 152.9 (C^a pyta), 149.6 (C^f pyta) 148.7 (C^e pyta), 140.9, 140.7 (PPh₃ C$_{meta}$), 139.7 (C^c pyta), 137.11, 137.07 (PPh₃ C$_{para}$), 130.9, 130.8 (PPh₃ C$_{ortho}$), 125.7 (C^d pyta), 122.6 (C^g pyta), 118.5, 117.4 (PPh₃), 54.0 (pyta-*C*H₂), 37.0 (NH-*C*H₂), 36.4 (NH-*C*H₂), 33.8 (NH-CH₂-*C*H₂), 21.6 (*C*H₃); ^{31}P NMR (121 MHz, CDCl₃): δ (ppm) 19.82; IR: 3224 (br, NH), 3037 (w, CH aromatic), 2922 (w, CH aliphatic), 2020 (S, CO A₁), 1910 (S, CO E), 1883 (S, CO E), 1670 (C=O amide); HRMS (ESI+): m/z calculated for [C₄₁H₄₄ClN₆O₅PRe]⁺: 953.2344 found: 953.2312; HPLC (5 to 100 % of acetonitrile in 10 min): t$_r$ = 8.52 min, purity > 85%.

Spectroscopy.

Fluorescence emission studies were performed on a Jasco spectrofluorometer FP-8300 in acetonitrile or MilliQ water (with 10% DMSO).

For luminescence quantum yields determination, fluorescence and absorbance spectra were recorded in acetonitrile (with 10% DMSO) at different concentrations for the three conjugates and in 0.1 N sulfuric acid solution for the reference quinine sulfate. For fluorescence spectra, the excitation was set at 330 nm and emission light was detected between 350 nm and 600 nm. Quinine sulfate in 0.1 N sulfuric acid was used as a standard with a known quantum yield of 54.6% (exc 320 nm).

The quantum yields were determined with the following equation:

$\phi_s = \phi_r \left(\dfrac{A_r}{A_s} \right) \left(\dfrac{F_s}{F_r} \right) \left(\dfrac{n^2_s}{n^2_r} \right)$ where the subscripts s and r refer to the sample and the standard

reference solution respectively; *n* is the refractive index of the solvents (the refractive index of 10% DMSO in acetonitrile was considered equal to that of acetonitrile); *F* is the integrated emission intensity; *A* is the absorbance at the excitation wavelength (A < 0.1) and ϕ is the luminescence quantum yield. The ratio F/A is given by the linear regressions.

Cell Culture.

A549 epithelial human lung carcinoma cells were cultured at 37 °C in a 5% CO₂ in air atmosphere. They were grown in high glucose DMEM with pyruvate sodium supplemented with 10% heat-

inactivated FBS and 1% penicillin/streptomycin.

Fluorescence Microscopy.

A549 cells were grown on glass coverslip to reach around 50% confluency and were then incubated for 4 hours in presence of the probes at 10 or 20 µM (final volume of DMSO $\leq$ 0,2%). At the end of the incubation, the medium was removed and a solution of fluorescent mitochondria tracker Mitotracker Deep Red (provided by Invitrogen) at 100 nM in complete media were added. After 30 minutes of incubation at 37 °C, the mitochondria staining solution were removed and the cells were washed twice with phosphate buffer. The cells were fixed with 4% para-formaldehyde for 8 min at room temperature and washed twice with PBS and once with milliQ water. Slides were air-dried and laid on a microscope slide with mounting media Vectashield (from Vector Laboratories) in between to minimize photobleaching and thus increase the sensitivity.

Fluorescence imaging was performed using an Olympus X71 microscope equipped with a C9100-02 camera (Hamamatsu Corporation, Sewickley, PA), a X60 oil-objective, a Lumencor Spectra X light source and a Hg lamp (100 W) attenuated by a neutral density filter. Microscopic slides were illuminated with the Hg lamp and luminescence signal of **C1**, **C2** and **C3** probes were detected using the following filter set: excitation D350/50x; beam splitter 400DCLP; emission HQ560/80m; Chroma Technology. For imaging, the glass coverslip (thinner part) was in contact with the oil. Microscopic slides were illuminated with the red source of Lumencor Spectra X and luminescence signal of the mitochondria tracker were detected using the appropriate filter set provided by Semrock (dichroic mirror: FF409/493/573/652-Di01-25x36 and emission filter: FF01-432/515/595/730-25). Image analysis was performed using Fiji software. The image background was subtracted using the "rolling ball" algorithm provided by Fiji.

The colocalization analysis were performed using the plugin coloc2 and JacoP implemented on Fiji software. The statistical confidence of the colocalization analysis results (Pearson value, Van-Steensel curve, scatter plot) were validated by the Costes' method. This method consists in randomizing the first image channel 200 times and to check that the Pearson coefficient is below that of the unrandomized image in 100% of cases.
The Van Steensel crosscorrelation function (CCF)[2] is a technique that shifts an image A on the x-axis pixel per pixel relative to another image B and calculate the respective Pearson Coefficient. A cross correlation function is obtained by plotting the Pearson coefficient as a function of the pixel shift dx. Complete colocalization shows a bell-shaped curve with maximum at dx = 0; partial colocalization shows a peak shifted from dx = 0. The CCF obtained for our conjugates show a partial overlay of the conjugates' labeling with that of the MitoTracker Deep Red.

Synchrotron Radiation X-ray Fluorescence (SXRF) Nano-imaging.

The intracellular distribution of rhenium in control cells and cells incubated with the probes was determined using SXRF nano-imaging. A549 cells were seeded on Si_3N_4 silicon nitride membranes (purchased from Silson Ltd, membrane size: 1.5 mm x 1.5 mm; membrane thickness: 500 nm) to reach around 50% confluency and treated with the probes at 20 µM (final volume of DMSO $\leq$

0,2%) for 4 hours at 37 °C under 5% CO_2. After incubation, they were washed twice with PBS, fixed with 4% paraformaldehyde, washed again twice with PBS and once with milliQ water and eventually air-dried.

The samples were examined on the hard X-ray nano-probe beamline, NANOSCOPIUM of the French national synchrotron facility, SOLEIL, Paris, France. Maps were recorded using a 14 keV incident beam energy. A549 cells were imaged by using a continuous scanning mode with a pixel size of 0.5 μm and with an accumulation time per pixel equal to 100, 200 or mostly 300 ms/pixel. Rapid scans were obtained beforehand at lower resolution (1 μm) and shorter dwell time (50 ms) to select the desired cells, previously located using phase- contrast optical microscopy. A total of 13 cells incubated with **C2** and **C3** probes and 9 cells incubated with **C1** were mapped. The full XRF spectra were collected in each pixel by two Si-drift detectors (Ketek) in order to increase the solid angle of detection.

The elemental calcium, phosphorus, rhenium and zinc distribution maps were extracted from the full XRF spectra using a MATLAB program developed by the NANOSCOPIUM team. For rhenium, the background was subtracted and for all elements, the maps were normalized to the dwell time per pixel allowing direct comparison across samples. The XRF sum-spectra extracted from the maps were processed by PyMCA.

The Cu-Kβ, Zn-Kα and Re-Lα lines at ~8.6 keV are 100 % overlapping. However, the good energy resolution of the XRF detectors of the Nanoscopium beamline ensures the unambiguous deconvolution of the Zn-Kβ (9.6 keV) and the Re-Lβ lines (~10.15 and 10.28 keV). As such, in order to avoid the eventual overlapping of Zn and Re signal in the Re images, we used only the Re-Lβ lines to create the X-ray intensity maps. The detailed description of the data treatment of the XRF data-set can be found in Hostachi *et al.*[3]

Quantification of rhenium accumulation in cells

The amount of Re accumulated in the cells were calculated by comparing the rhenium signal summed within a mask of the mapped cells to the rhenium signal of a rhenium external standard. Masks of the cells were determined from the calcium map or the phosphorus spectra map. The Re standard was prepared by depositing 0.3 μL of a 10 μM solution of $Re(CO)_5Cl$ in MeOH (3.0 x 10^{-12} mol) on a silicon nitride SiN_3 membrane. The membrane was air-dried and the imaging of this rhenium standard (pixel size = 1 μm and integration time = 10 ms, Figure S27) allows us to identify the whole area of the Re droplet and to calculate precisely the total Re intensity, 2.32 x 10^7 I_{fluo}/s corresponding to the deposited rhenium molar quantity (3.0 x 10^{-12} mol) within the droplet by fitting the Re spectrum by PyMCA. This permits to calculate the conversion factor between the measured Re XRF intensity and molar concentrations, which is: 1.29 x 10^{-19} $mol.s/I_{fluo}$.

Cytotoxicity Assay

The probes cytotoxicity was assessed by using the MTT (3-(4,5-dimethylthiazol-2-yl)-2,5-diphenyltetrazolium bromide) assay based on the mitochondrial-dependent reduction of MTT to

formazan. A549 cells were grown in 96-well plate to reach around 90% confluency and were then incubated for 4 hours at 37 °C in the presence of the probes at concentrations varying between 1 µM and 1 mM. The medium was then removed; the cells were washed with PBS and were incubated with a solution of MTT at 0.5 mg/mL for two hours at 37 °C. At the end of the incubation, formazan crystals were visible under the microscope. Three quarters of the MTT solution were removed in each well and were replaced by DMSO. The plate was incubated for 30 minutes at 37 °C to solubilize the formazan crystals. After complete solubilization of the formazan crystals, the extent of reduction of MTT to formazan by the cells was quantified by the measurement of the absorbance at 570 nm. A blank without cells were included in order to subtract the background corresponding to the culture medium from all samples. The percentage of cell viability compared to the untreated control were then calculated and were plotted as a function of the probe concentration. IC50 were calculated by fitting this curve with a four-parameter logistic curve using the Matlab L4P regression function. The MTT assay was performed for two biological replicates. For each biological replicate, the compounds' cytotoxicity was screened at each concentration in triplicate.

Results
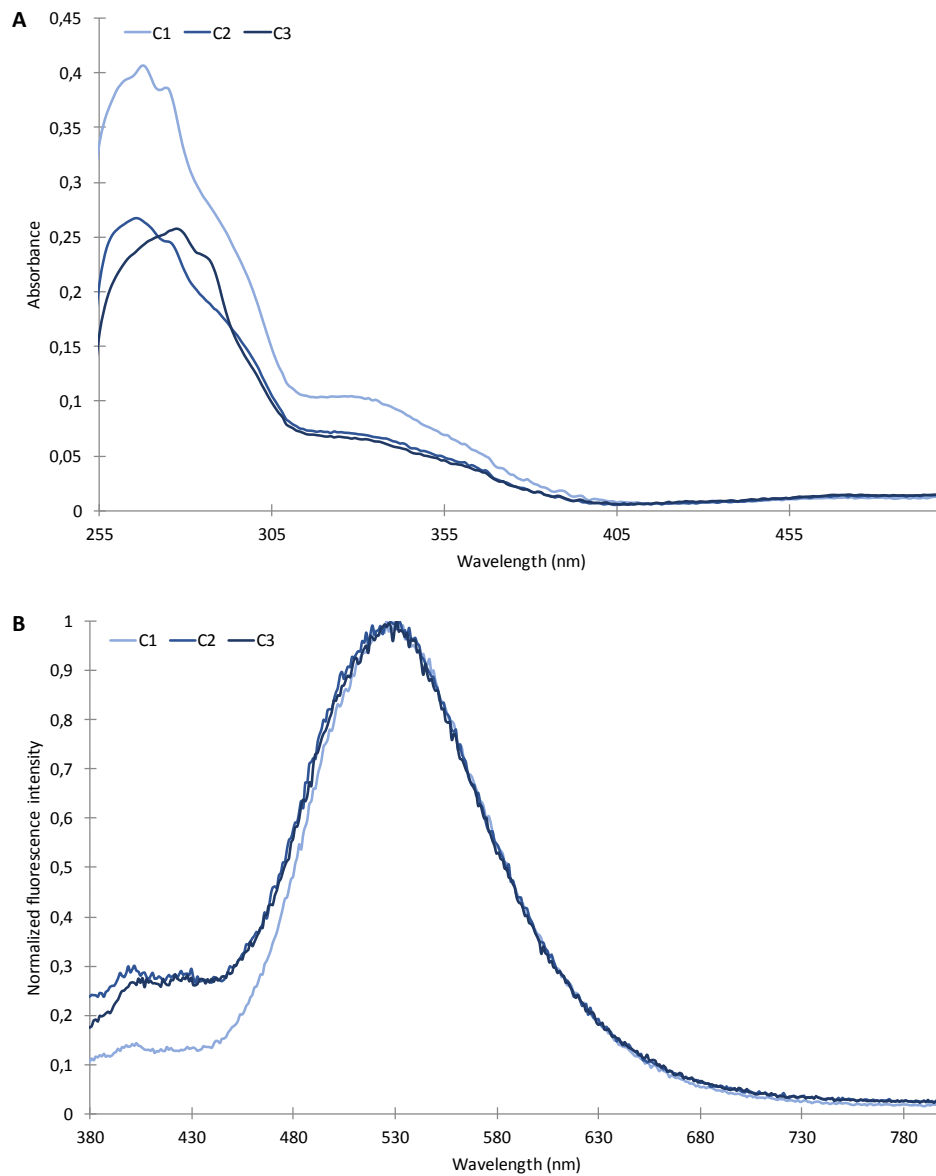
Figure S1. A. UV-vis absorption spectra of complexes **C1-C3** in acetonitrile (with 10% DMSO, 20 μM); **B.** Normalized luminescence emission spectra of complexes **C1-C3** (20 μM) in acetonitrile (with 10% DMSO) (λexc 330 nm).
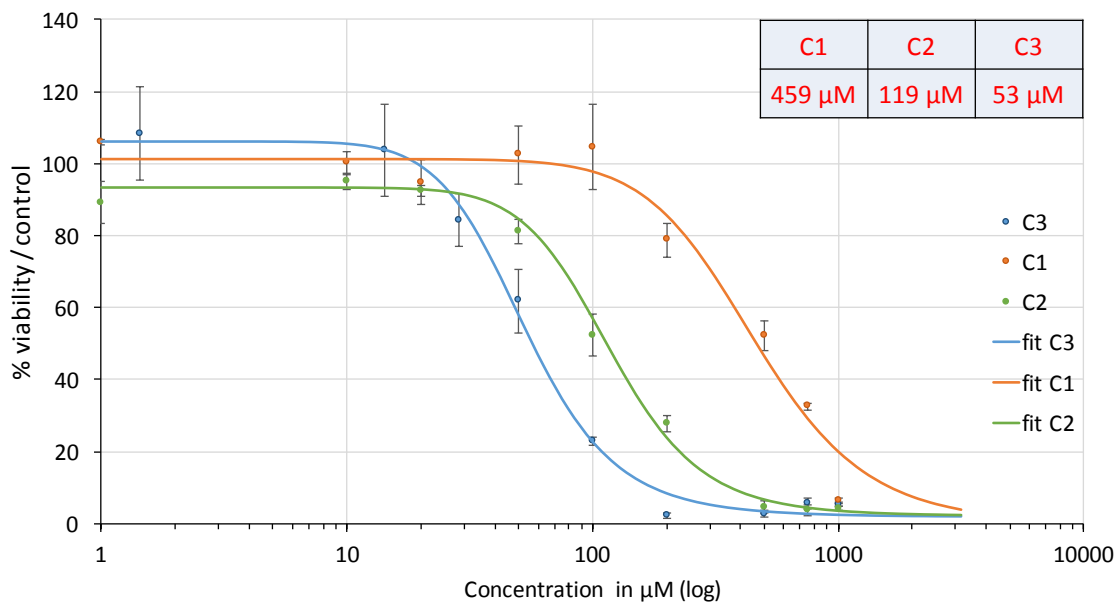
Fig. S2. Example of determination of IC50. The cytotoxicity of the three probes were assessed from the MTT assay at concentrations varying between 1 µM and 1 mM. IC50 were calculated by fitting the plot of cell survival (%) versus probe concentration (µM) with a four-parameter logistic curve. The curves represented here correspond to one biological replicate and each dot to the mean of technical triplicates.

	IC50 (µM)
C1	413 ± 65
C2	100 ± 26
C3	46 ± 10
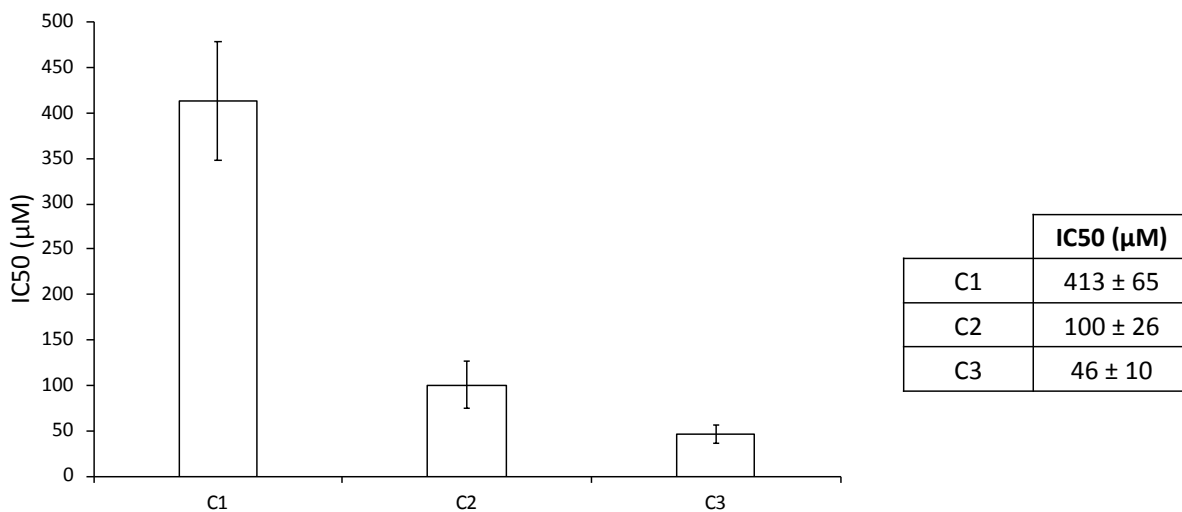
Figure S3. Probe concentrations that produce 50 % cell growth inhibition (IC50). IC50 were calculated from curves constructed by plotting cell survival (%) versus probe concentration (µM). The percentage of cell survival was calculated at each concentration using the MTT viability assay. The MTT assay was performed for two biological replicates. For each biological replicate, the compounds cytotoxicity was screened at each concentration in triplicate.

11
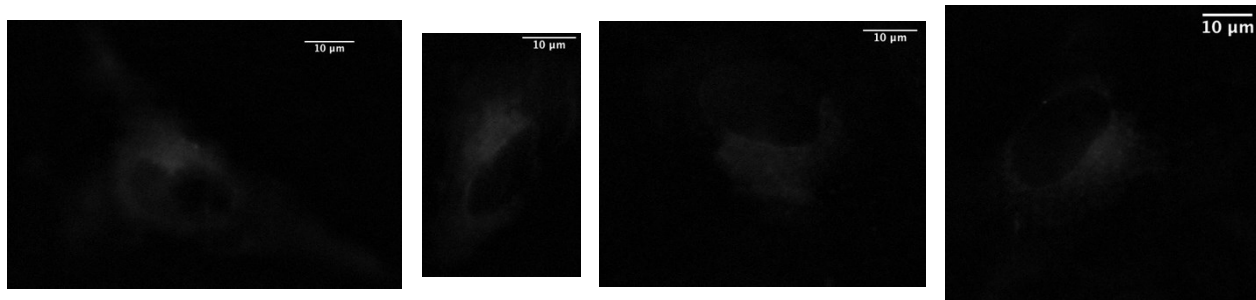
Figure S4. Fluorescence imaging of A549 control cells (excitation 350 nm). The signal-to-noise ratio were equal to 23.5 dB, 22.9 dB, 22.0 dB and 22.3 dB respectively. Fixed fluorescence intensity scale (0-7500 u.a). Scale bar: 10 µm (fixed at 1.55 cm).
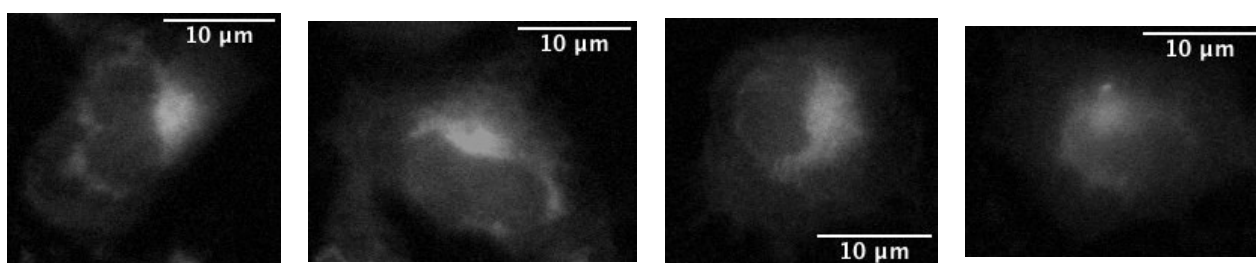
Figure S5. Fluorescence imaging of A549 cells incubated with conjugate **C1** (at 20 µM for 4 h) (excitation 350 nm). The signal-to-noise ratio were equal to 32.9 dB, 32.5 dB, 33.3 dB and 30.9 dB respectively. Fixed fluorescence intensity scale (0-7500 u.a). Scale bar: 10 µm (fixed at 3.1 cm).
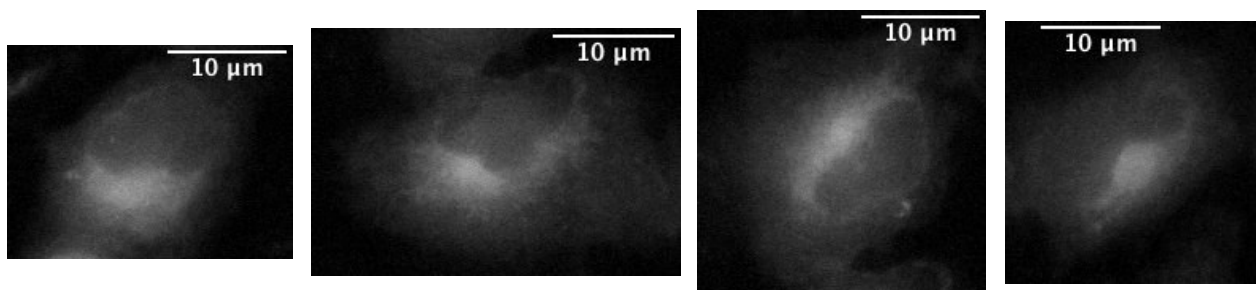
Figure S6. Fluorescence imaging of A549 cells incubated with conjugate **C2** (at 20 µM for 4 h) (excitation 350 nm). The signal-to-noise ratio were equal to 32.5 dB, 33.1 dB, 35.0 dB and 33.4 dB respectively. Fixed fluorescence intensity scale (0-7500 u.a). Scale bar: 10 µm (fixed at 3.1 cm).
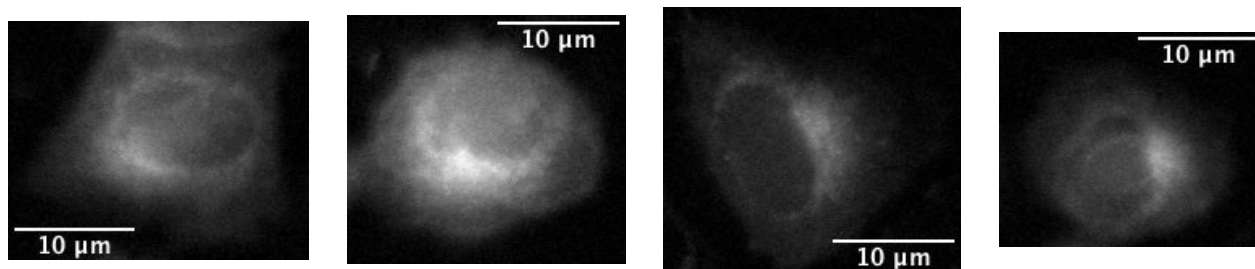
Figure S7. Fluorescence imaging of A549 cells incubated with conjugate **C3** (at 20 µM for 4 h) (excitation 350 nm). The signal-to-noise ratio were equal to 34.5 dB, 35.4 dB, 33.4 dB and 36.5 dB respectively. Fixed fluorescence intensity scale (0-7500 u.a). Scale bar: 10 µm (fixed at 3.1 cm).
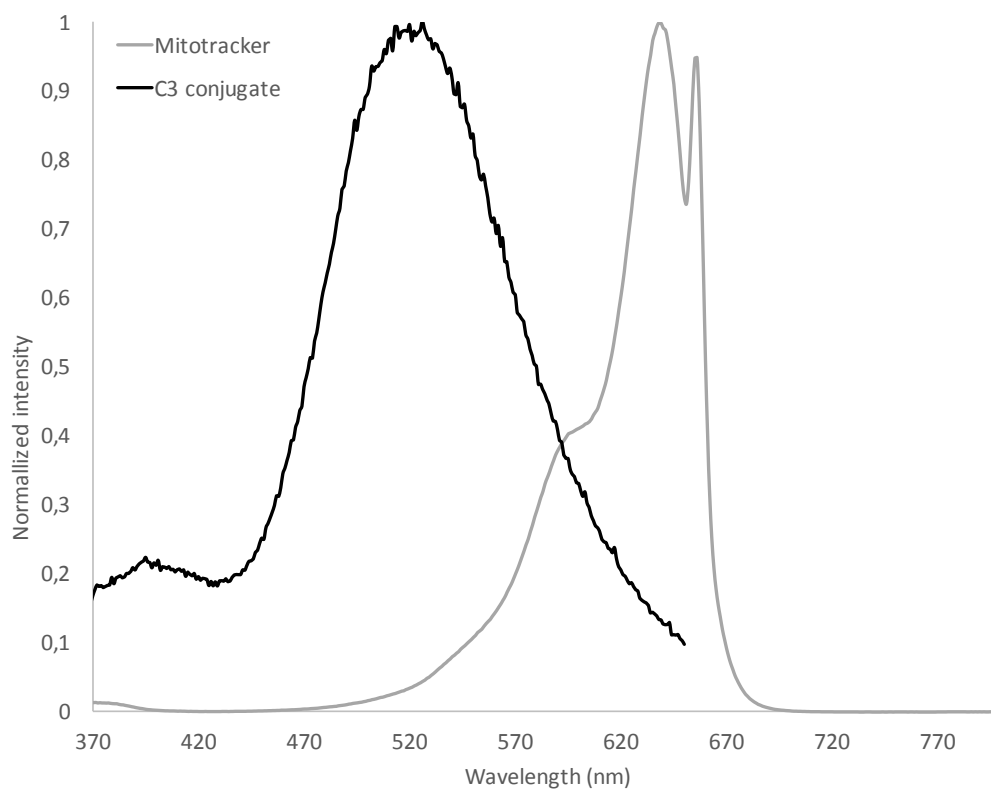
Figure S8. Normalized luminescence emission spectrum of **C3** conjugate (50 µM, in H_2O/DMSO 90/10 v/v, black curve) (λexc 320 nm) and excitation spectrum of Mitotracker Deep Red (100 nM in H_2O) (λem 657 nm).
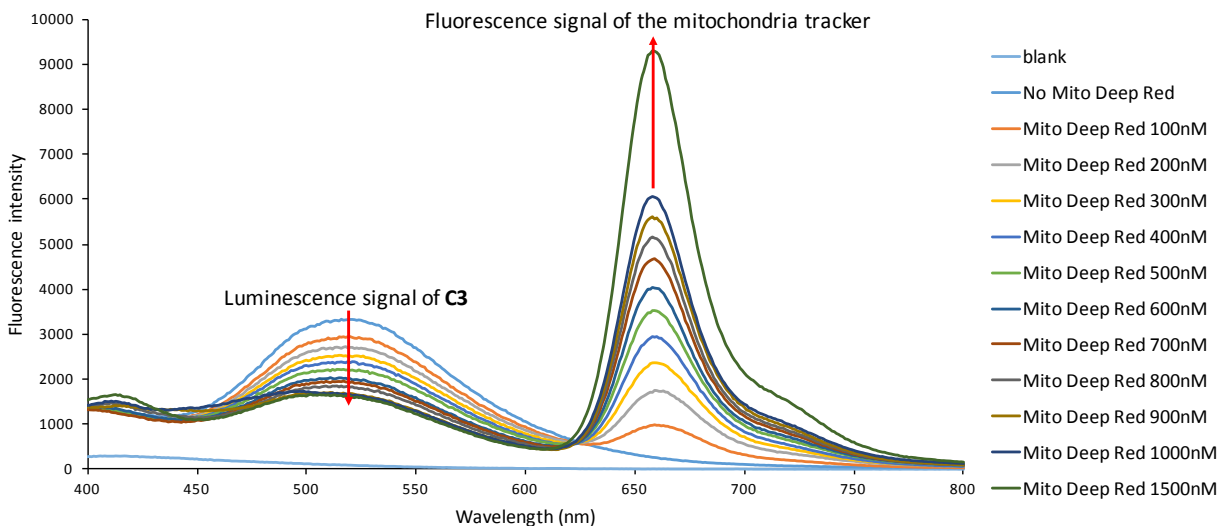
Fig S9. Effect of mitochondria tracker co-incubation on the luminescence signal of the C3 probe. The **C3** probe was prepared at 50 μM in MilliQ water (with 10% DMSO). The mitochondria tracker Mitotracker Deep Red was added to the **C3** solution at concentrations varying between 100 nM and 1500 nM. Fluorescence spectra were recorded by exciting at 320 nm and detecting emission light between 400 nm and 800 nm.
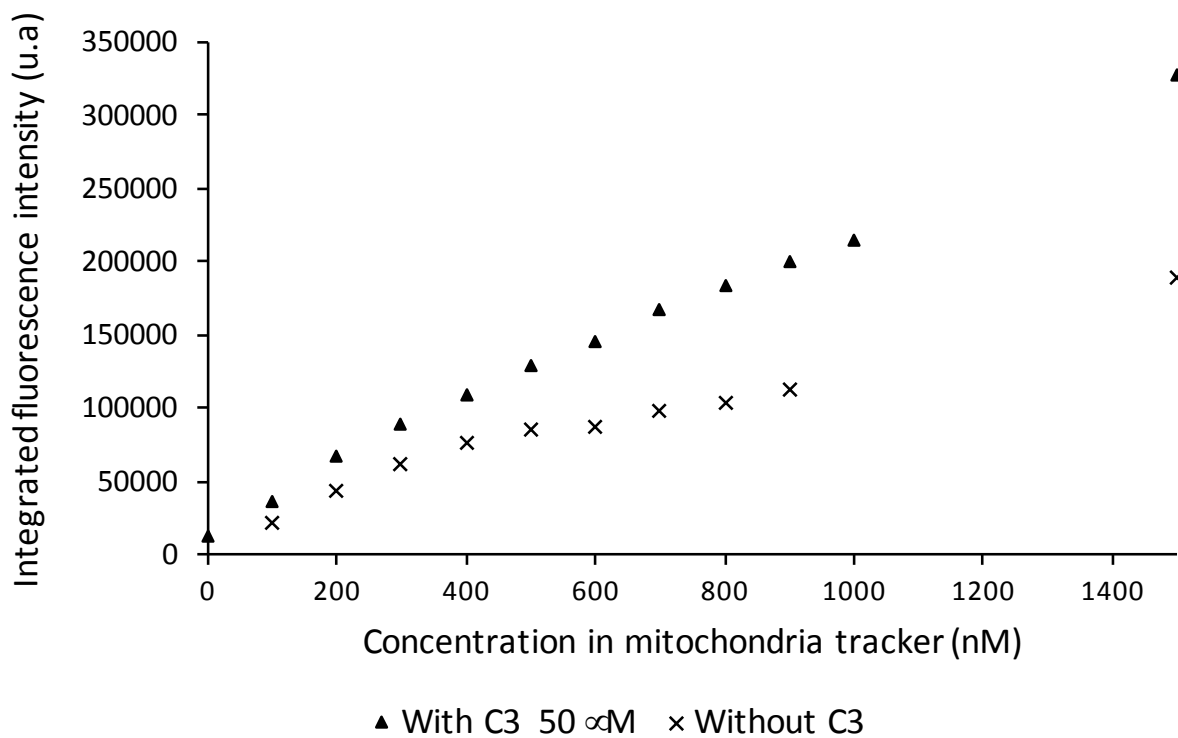
Fig. S10. Integrated fluorescence intensity (635 to 685 nm) of a solution of the mitochondria

tracker in presence or not of **C3** at 50 µM, upon excitation at 320 nm. The fluorescence intensity of the mitochondria tracker is higher when co-incubated with **C3**. This result suggests the existence of fluorescence resonance energy transfer between the two compounds.
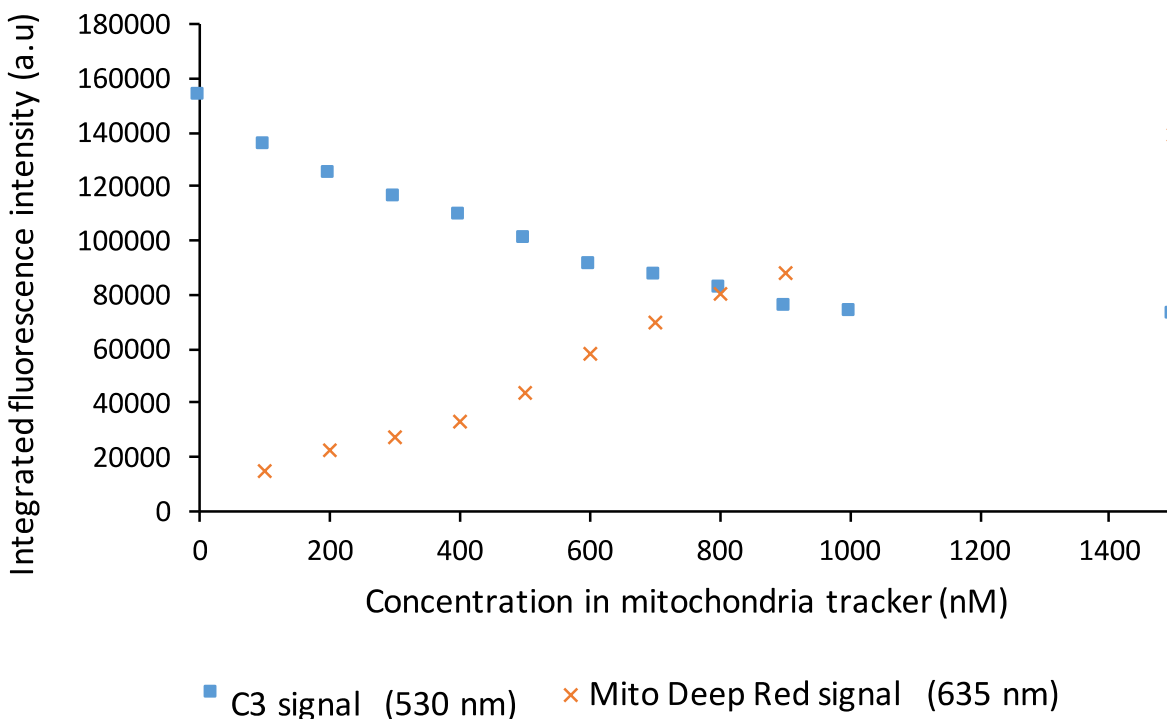
Fig S11. Effect of the co-incubation of **C3** with the mitochondria tracker on their respective fluorescence intensity. **C3** integrated luminescence intensity (500 - 550 nm) (50 µM in MilliQ water, λexc 320 nm) was plotted as a function of the concentration of mitochondria tracker. The integrated fluorescence intensity of the mitochondria tracker co-incubated with **C3** was subtracted by that of the mitochondria tracker at the same concentration without **C3** and plotted as a function of the mitochondria tracker concentration.
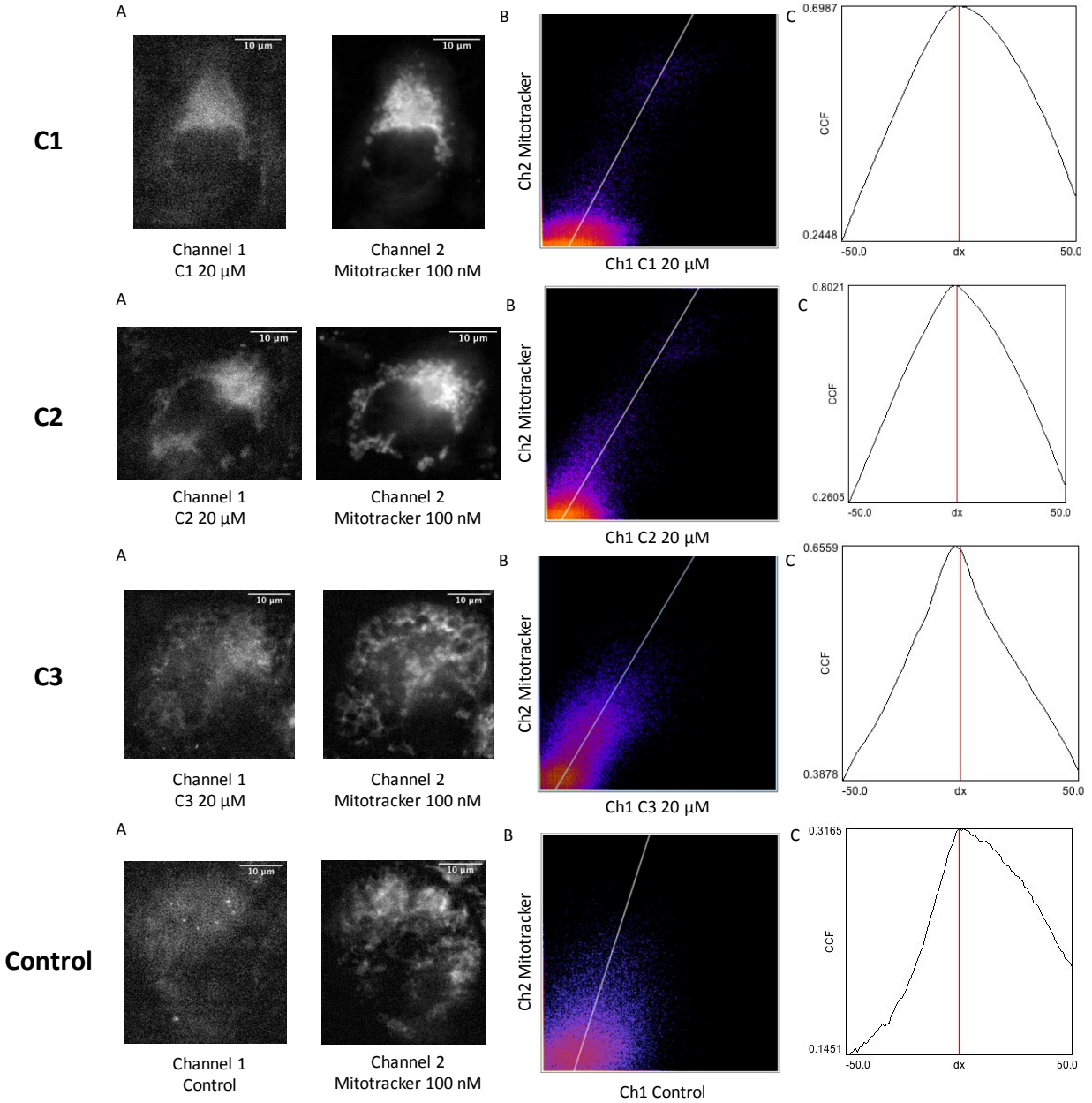
Figure S12. Colocalization analyses with the fluorescence signal of Mitotracker Deep Red. A549 cells were incubated with **C1-C3** probes at 20 µM for 4 hours or without incubation (control). (A) Left: channel 1 – fluorescence image with excitation at λexc 350 nm, obtained with a gain of 0 over an exposure time of 3s. The signal-to-noise ratio is equal to 17dB for **C1**, 24 dB for **C2**, 23 dB for **C3** and 10 dB for control cells; Right: channel 2 – fluorescence image of the Mitotracker Deep Red (λexc 644 nm) obtained with a gain of 0 over an exposure time of 5s. (B) Scatter plot or 2D-histogram with a linear regression representing the signal intensity relationship of the two fluorescence images. (C) Van Steensel curve. The cross correlation function is maximal for a shift dx equal to 0, 1, 2 and 0 pixels for **C1**, **C2**, **C3** and control cells, respectively. The Pearson coefficient is equal to 0.70 for **C1**, 0.80 for **C2**, 0.66 for **C3** and 0.32 for control cells.

C1
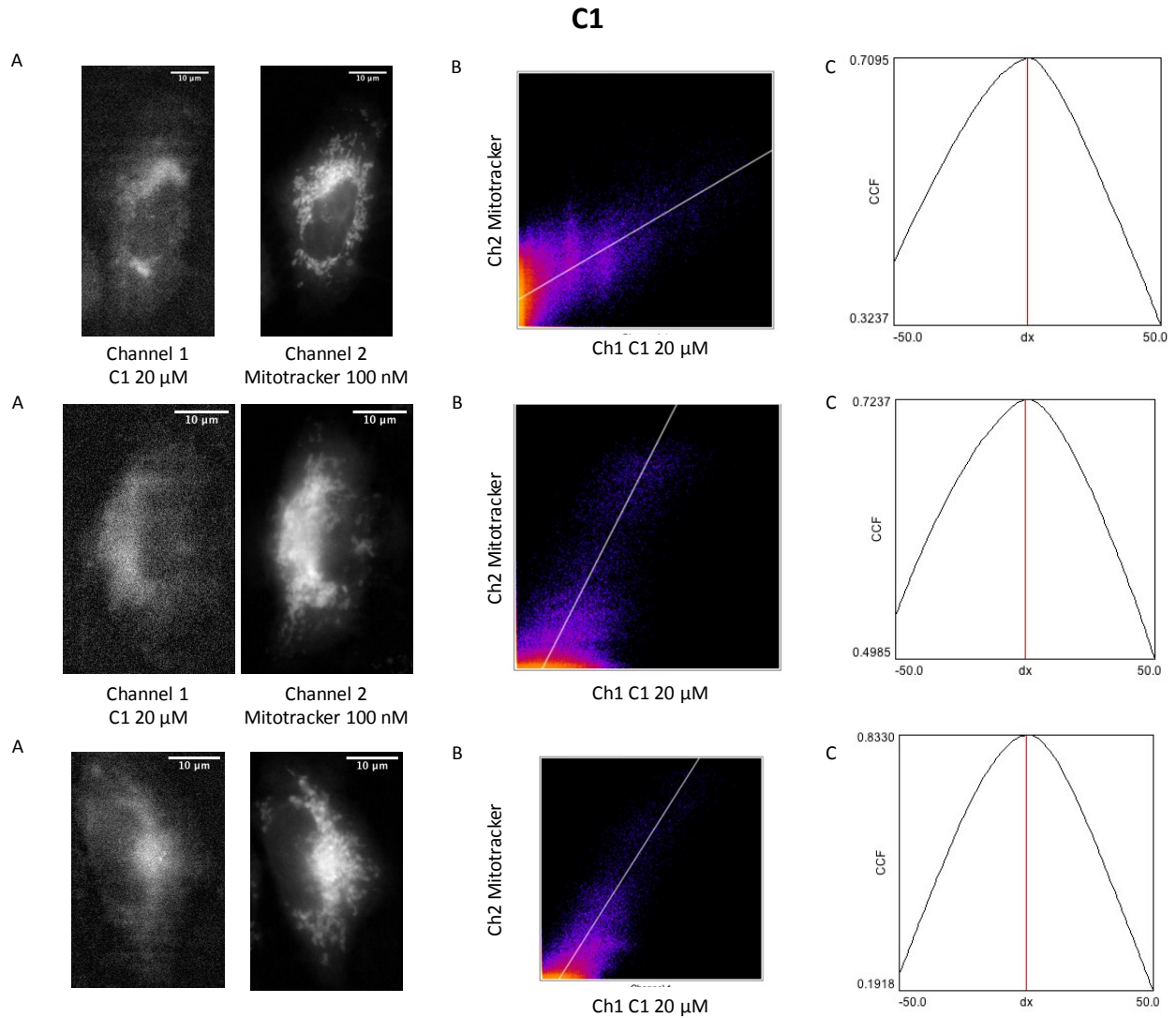
Figure S13. Colocalization analyses with the fluorescence signal of Mitotracker Deep Red. A549 cells were incubated with **C1** probe at 20 μM for 4 hours. (A) Left: channel 1 – fluorescence image with excitation at λexc 350 nm, obtained with a gain of 0 over an exposure time of 3s. The signal-to-noise ratio is equal to 16.9 dB; Right: channel 2 – fluorescence image of the Mitotracker Deep Red (λexc 644 nm) obtained with a gain of 0 over an exposure time of 5s. (B) Scatter plot or 2D-histogram with a linear regression representing the signal intensity relationship of the two fluorescence images. (C) Van Steensel curve. The cross correlation function is maximal for a shift dx equal to 1, 2 and 2 pixels, respectively. The Pearson coefficient is equal to 0.71, 0.72, 0.83 respectively.

C2
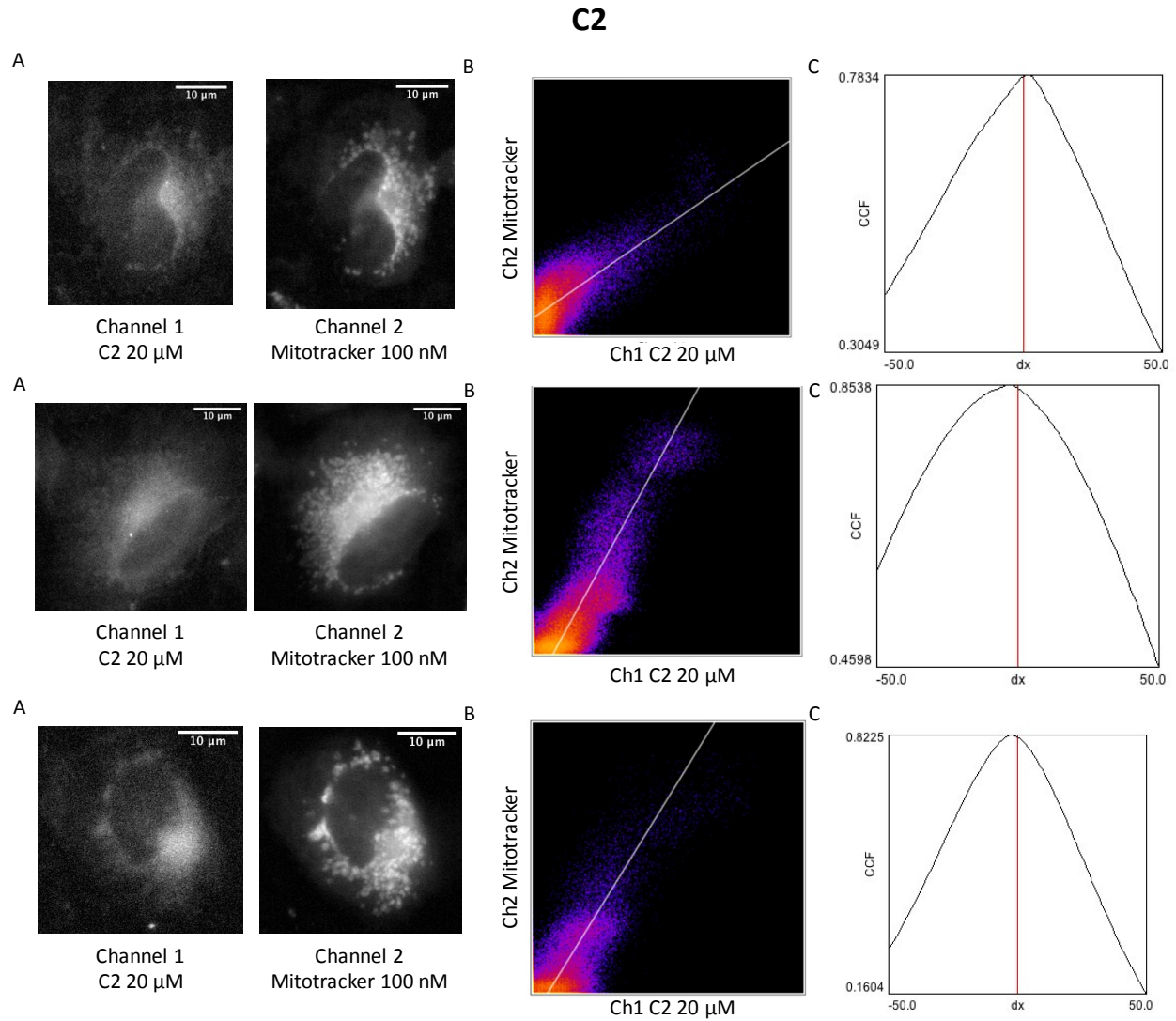
Figure S14. Colocalization analyses with the fluorescence signal of Mitotracker Deep Red. A549 cells were incubated with **C2** probe at 20 µM for 4 hours. (A) Left: channel 1 – fluorescence image with excitation at λexc 350 nm, obtained with a gain of 0 over an exposure time of 3s. The signal-to-noise ratio is equal to 19 dB and 20 dB respectively; Right: channel 2 – fluorescence image of the Mitotracker Deep Red (λexc 644 nm) obtained with a gain of 0 over an exposure time of 5s. (B) Scatter plot or 2D-histogram with a linear regression representing the signal intensity relationship of the two fluorescence images. (C) Van Steensel curve. The cross correlation function is maximal for a shift dx equal to 2, 3 and 3 pixels, respectively. The Pearson coefficient is equal to 0.78, 0.85, 0.82 respectively.

C3
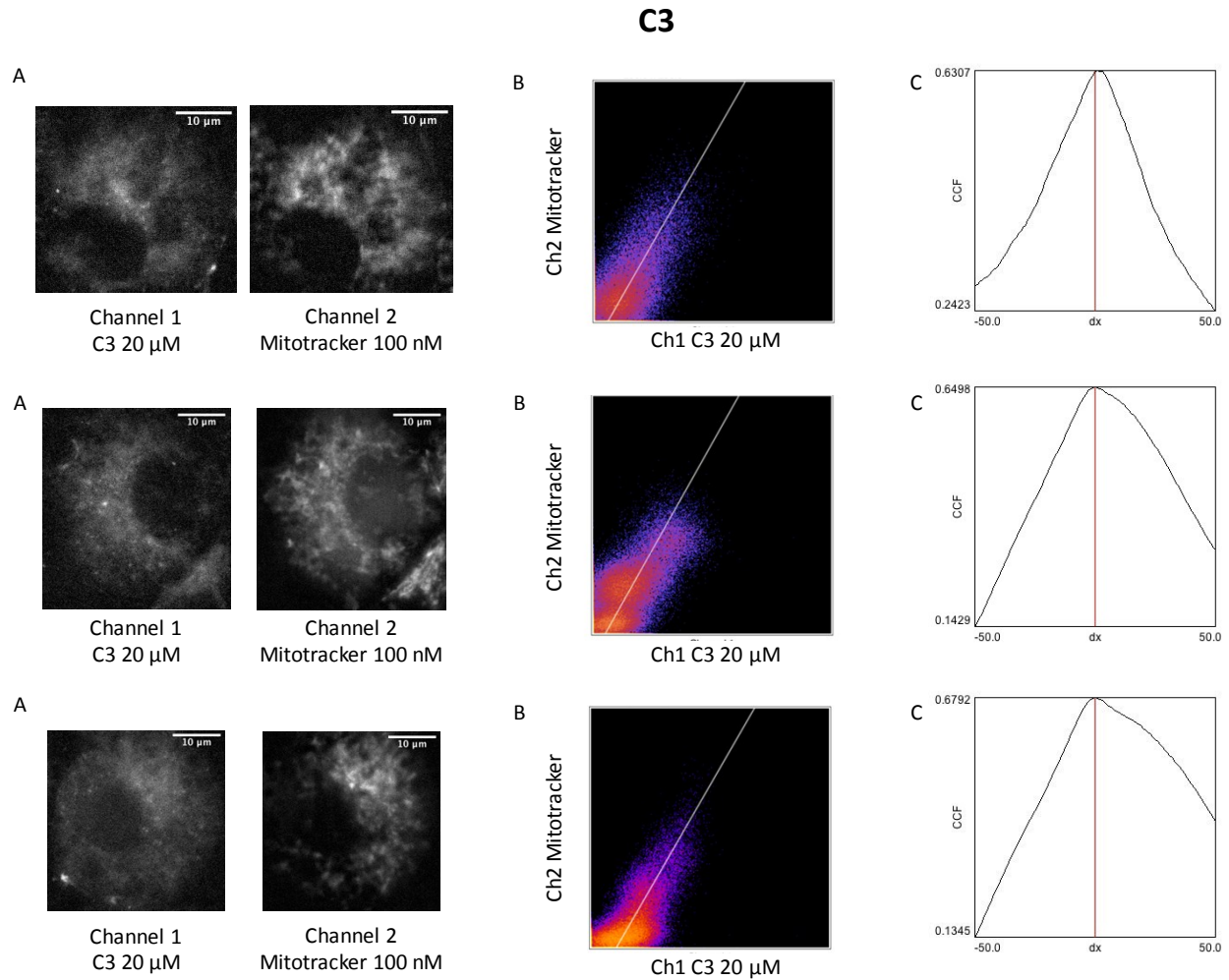
Figure S15. Colocalization analyses with the fluorescence signal of Mitotracker Deep Red. A549 cells were incubated with **C3** probe at 20 µM for 4 hours. (A) Left: channel 1 – fluorescence image with excitation at λexc 350 nm, obtained with a gain of 0 over an exposure time of 3s. The signal-to-noise ratio is equal to 19.2 dB; Right: channel 2 – fluorescence image of the Mitotracker Deep Red (λexc 644 nm) obtained with a gain of 0 over an exposure time of 5s. (B) Scatter plot or 2D-histogram with a linear regression representing the signal intensity relationship of the two fluorescence images. (C) Van Steensel curve. The cross correlation function is maximal for a shift dx equal to 2, 0 and 0 pixels, respectively. The Pearson coefficient is equal to 0.63, 0.65, 0.68 respectively.
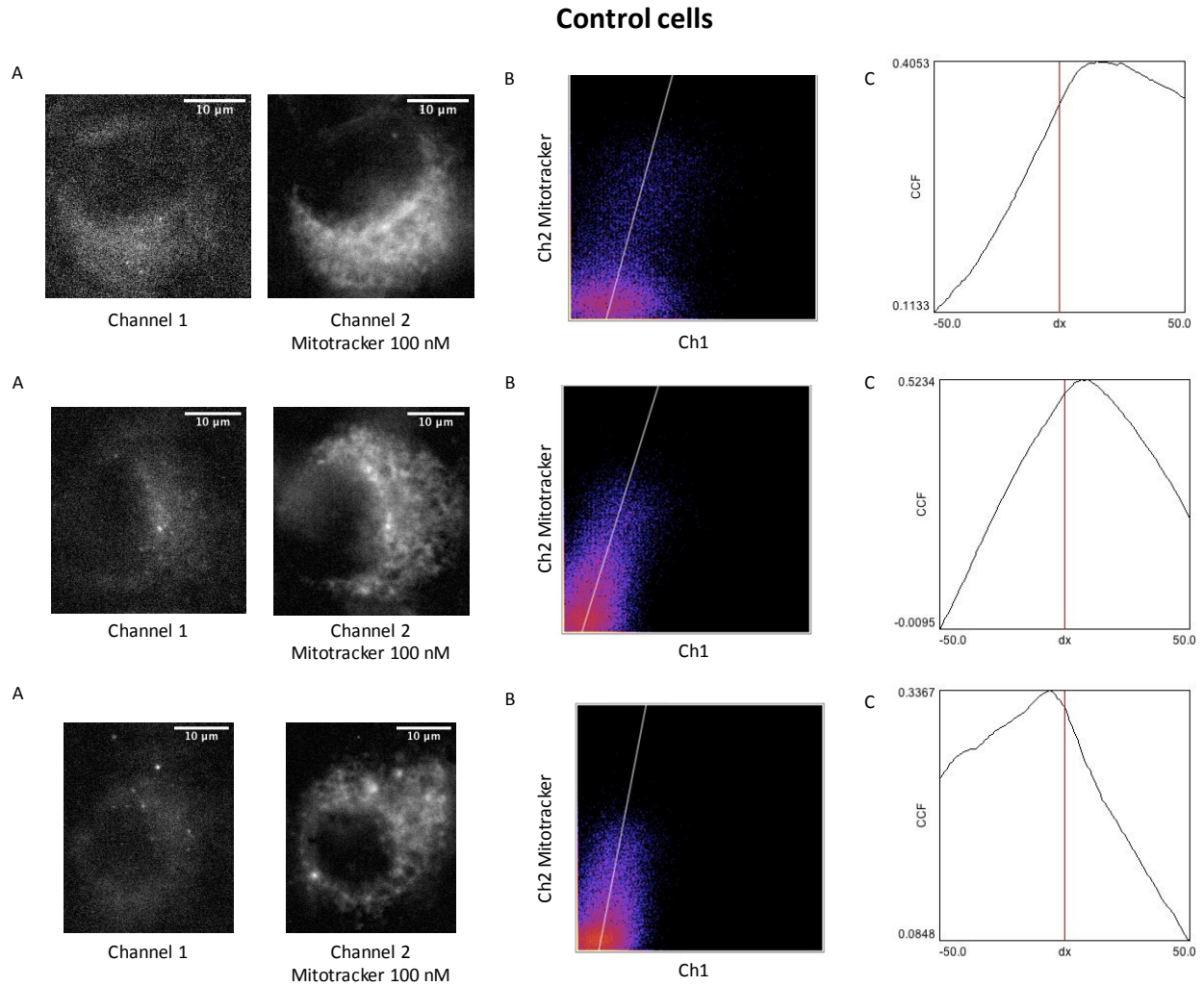
Control cells

Figure S15. A549 control cells in colocalization analyses with the fluorescence signal of Mitotracker Deep Red. (A) Left: channel 1 - fluorescence image with excitation at λexc 350 nm, obtained with a gain of 0 over an exposure time of 3s. The signal-to-noise ratio is equal to 12.9 dB; Right: channel 2 – fluorescence image of the Mitotracker Deep Red (λexc 644 nm) obtained with a gain of 0 over an exposure time of 5s. (B) Scatter plot or 2D-histogram with a linear regression representing the signal intensity relationship of the two fluorescence images. (C) Van Steensel curve. The cross correlation function is maximal for a shift dx equal to 17, 8 and 6 pixels, respectively. The Pearson coefficient is equal to 0.36, 0.50, 0.32 respectively.
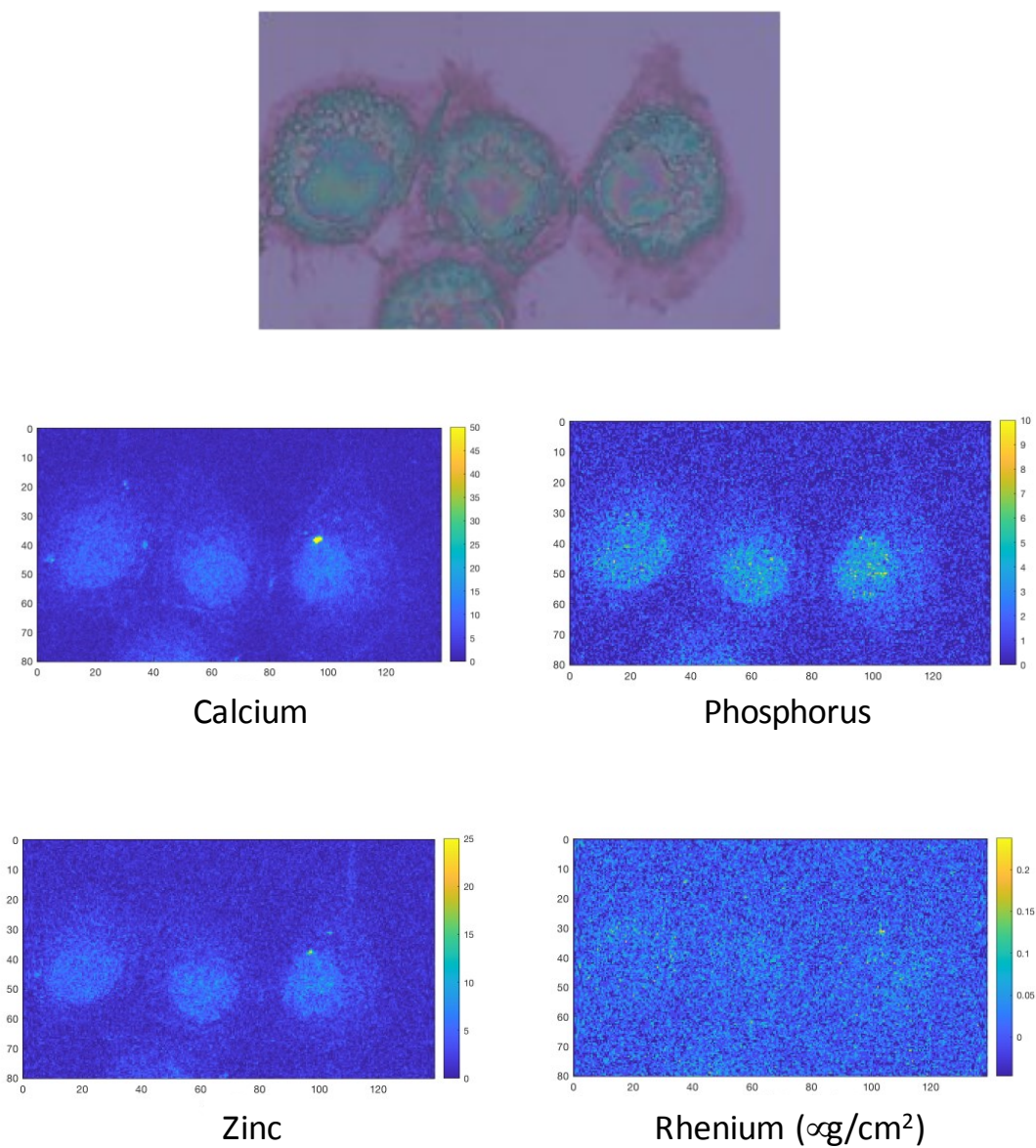
Figure S16. Elemental distributions of Ca, P, Re, and Zn in A549 cells incubated with **C1** (with color map (intensity) (right) and corresponding transmission optical microscope image (top). The phosphorus (P), and zinc (Zn, Kβ-lines) maps are used to identify the nucleus area. Re was mapped using the Lß lines (~10.15 and 10.28 keV). A549 cells were incubated for 4 hours with **C1** (20 μM) before fixation and air-drying (excitation at 14 keV; integration time, 300 ms per pixel; pixel size, 500 nm). Scale axis in μm.

Calcium

Phosphorus

Zinc

Rhenium (∝g/cm²)
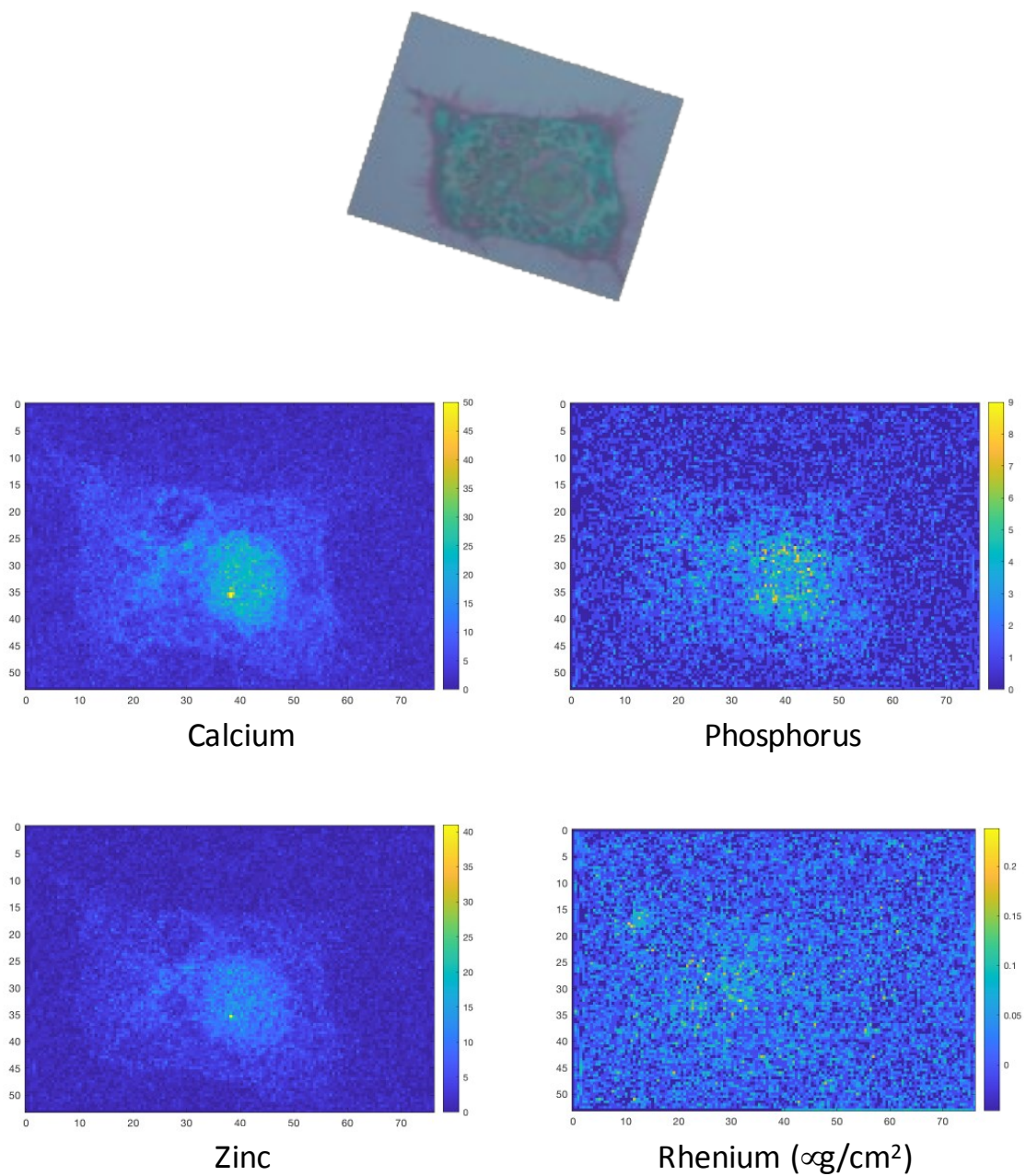
Figure S17. Elemental distributions of Ca, P, Re, and Zn in A549 cells incubated with **C1** (with color map (intensity) (right) and corresponding transmission optical microscope image (top). The phosphorus (P), and zinc (Zn, Kβ-lines) maps are used to identify the nucleus area. Re was mapped using the Lß lines (~10.15 and 10.28 keV). A549 cells were incubated for 4 hours with **C1** (20 μM) before fixation and air-drying (excitation at 14 keV; integration time, 300 ms per pixel; pixel size, 500 nm). Scale axis in μm.

Calcium

Phosphorus

Zinc

Rhenium ($\propto$g/cm^2)
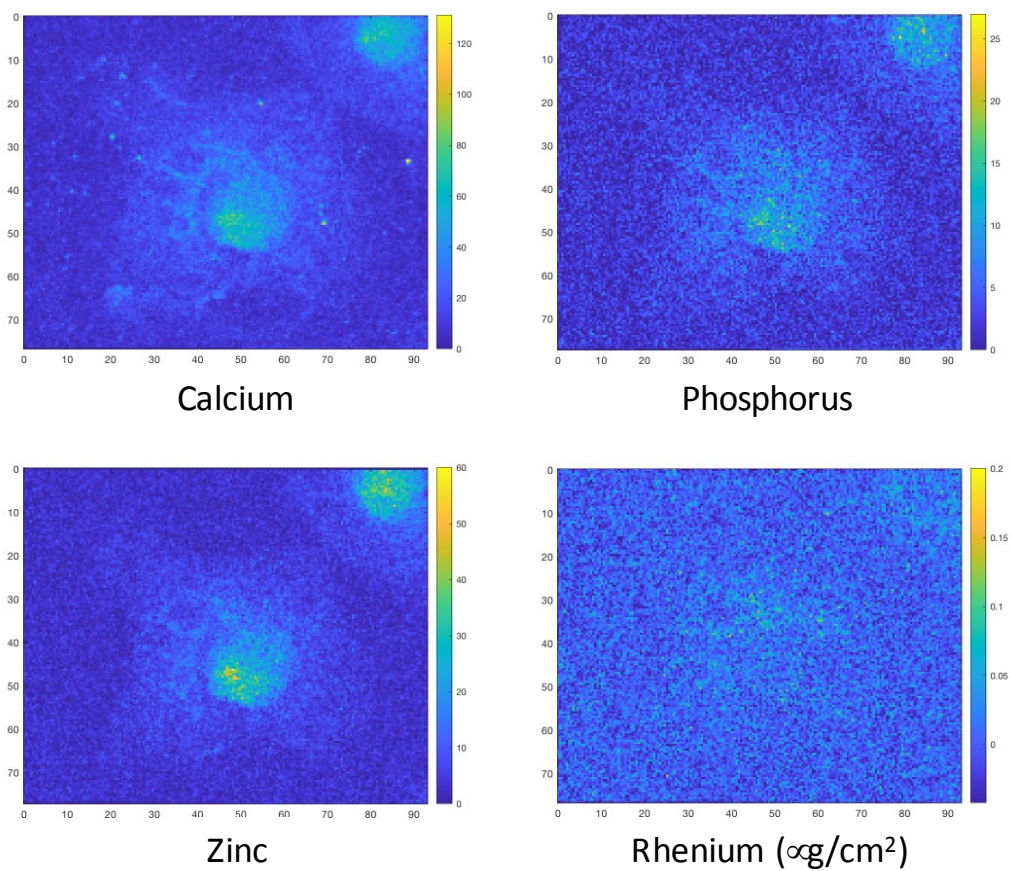
Figure S18. Elemental distributions of Ca, P, Re, and Zn in A549 cells incubated with **C1** (with color map (intensity) (right). The phosphorus (P), and zinc (Zn, Kβ-lines) maps are used to identify the nucleus area. Re was mapped using the Lß lines (~10.15 and 10.28 keV). A549 cells were incubated for 4 hours with **C1** (20 μM) before fixation and air-drying (excitation at 14 keV; integration time, 300 ms per pixel; pixel size, 500 nm). Scale axis in μm.
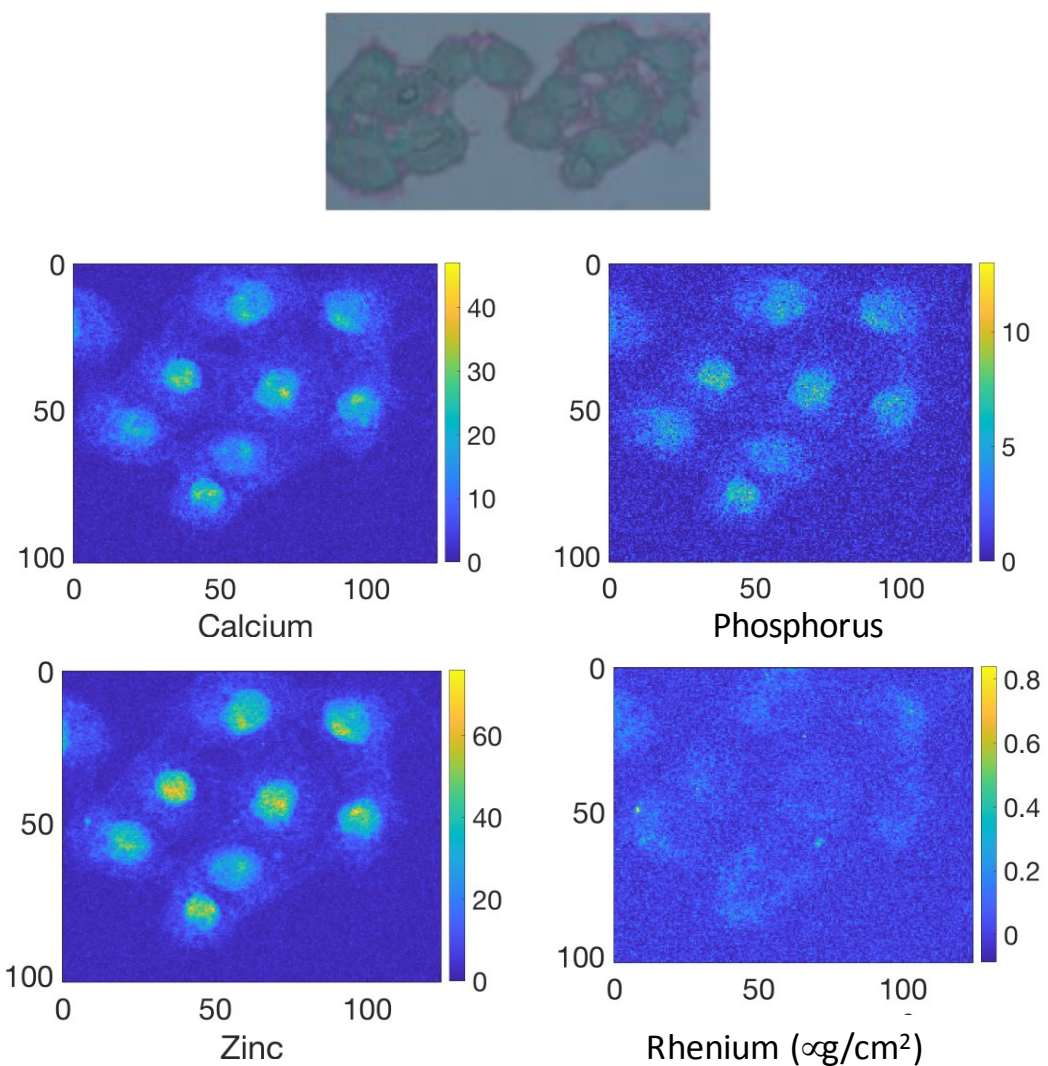
Figure S19. Elemental distributions of Ca, P, Re, and Zn in A549 cells incubated with **C2** (with color map (intensity) (right) and corresponding transmission optical microscope image (top). The phosphorus (P), and zinc (Zn, Kβ-lines) maps are used to identify the nucleus area. Re was mapped using the Lß lines (~10.15 and 10.28 keV). A549 cells were incubated for 4 hours with **C2** (20 μM) before fixation and air-drying (excitation at 14 keV; integration time, 300 ms per pixel; pixel size, 500 nm). Scale axis in μm.
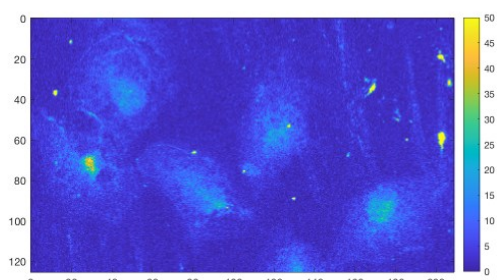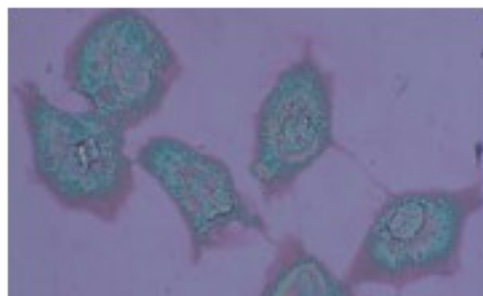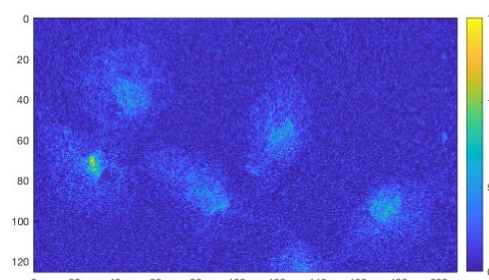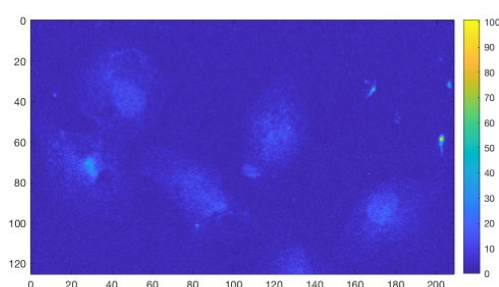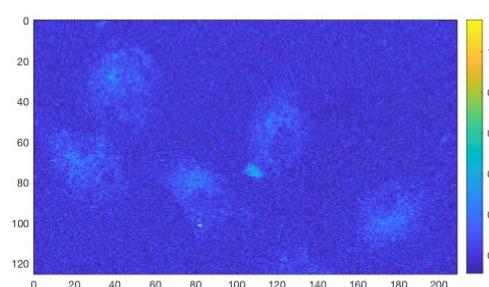
Figure S20. Elemental distributions of Ca, P, Re, and Zn in A549 cells incubated with **C3** (with color map (intensity) (right) and corresponding transmission optical microscope image (top). The phosphorus (P), and zinc (Zn, Kβ-lines) maps are used to identify the nucleus area. Re was mapped using the Lß lines (~10.15 and 10.28 keV). A549 cells were incubated for 4 hours with **C3** (20 μM) before fixation and air-drying (excitation at 14 keV; integration time, 300 ms per pixel; pixel size, 500 nm). Scale axis in μm.
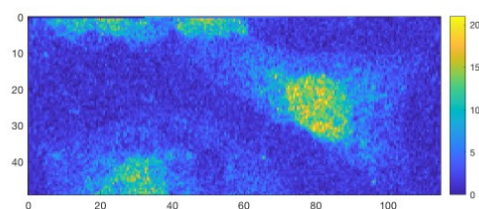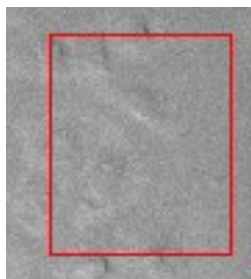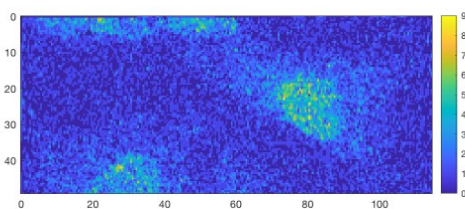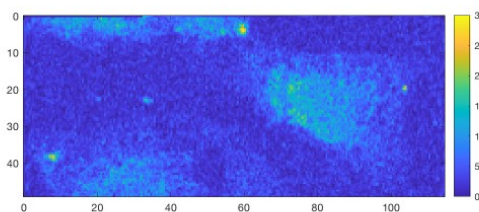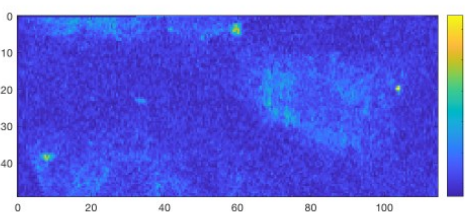
Figure S21. Elemental distributions of Ca, P, Re, and Zn in A549 cells incubated with **C3** (with color map (intensity) (right) and corresponding transmission optical microscope image (top). The phosphorus (P), and zinc (Zn, Kβ-lines) maps are used to identify the nucleus area. Re was mapped using the Lß lines (~10.15 and 10.28 keV). A549 cells were incubated for 4 hours with **C3** (20 μM) before fixation and air-drying (excitation at 14 keV; integration time, 300 ms per pixel; pixel size, 500 nm). Scale axis in μm.

Calcium

Phosphorus

Zinc

Rhenium (∝g/cm²)
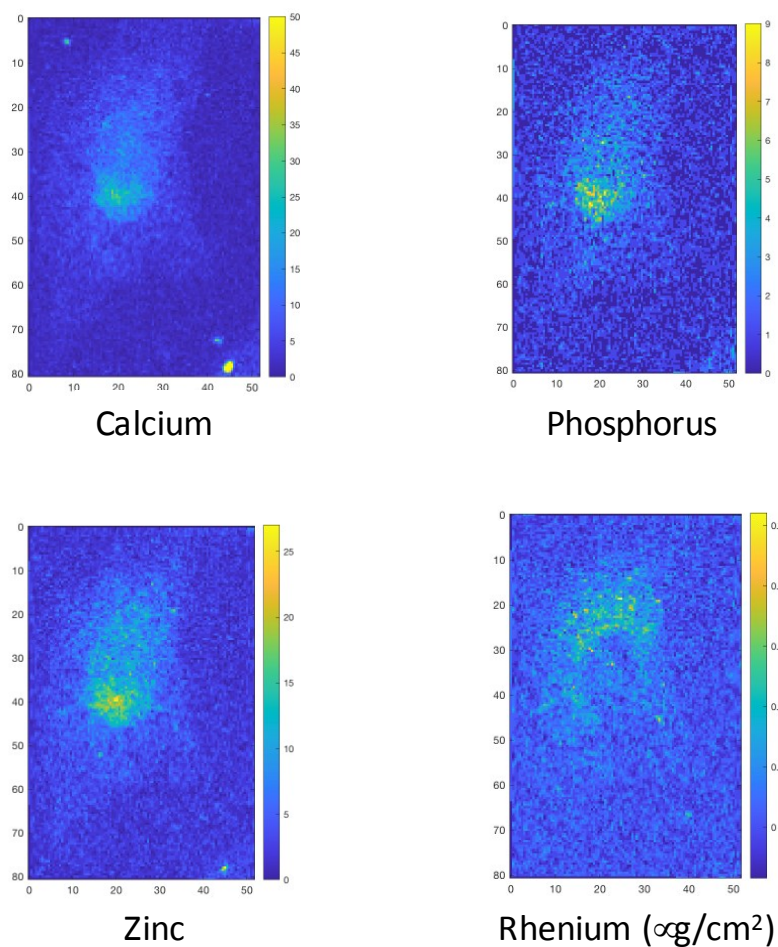
Figure S22. Elemental distributions of Ca, P, Re, and Zn in A549 cells incubated with **C3** (with color map (intensity) (right). The phosphorus (P), and zinc (Zn, Kβ-lines) maps are used to identify the nucleus area. Re was mapped using the Lß lines (~10.15 and 10.28 keV). A549 cells were incubated for 4 hours with **C3** (20 μM) before fixation and air-drying (excitation at 14 keV; integration time, 300 ms per pixel; pixel size, 500 nm). Scale axis in μm.

Calcium

Phosphorus

Zinc

Rhenium ($\propto$g/cm^2)
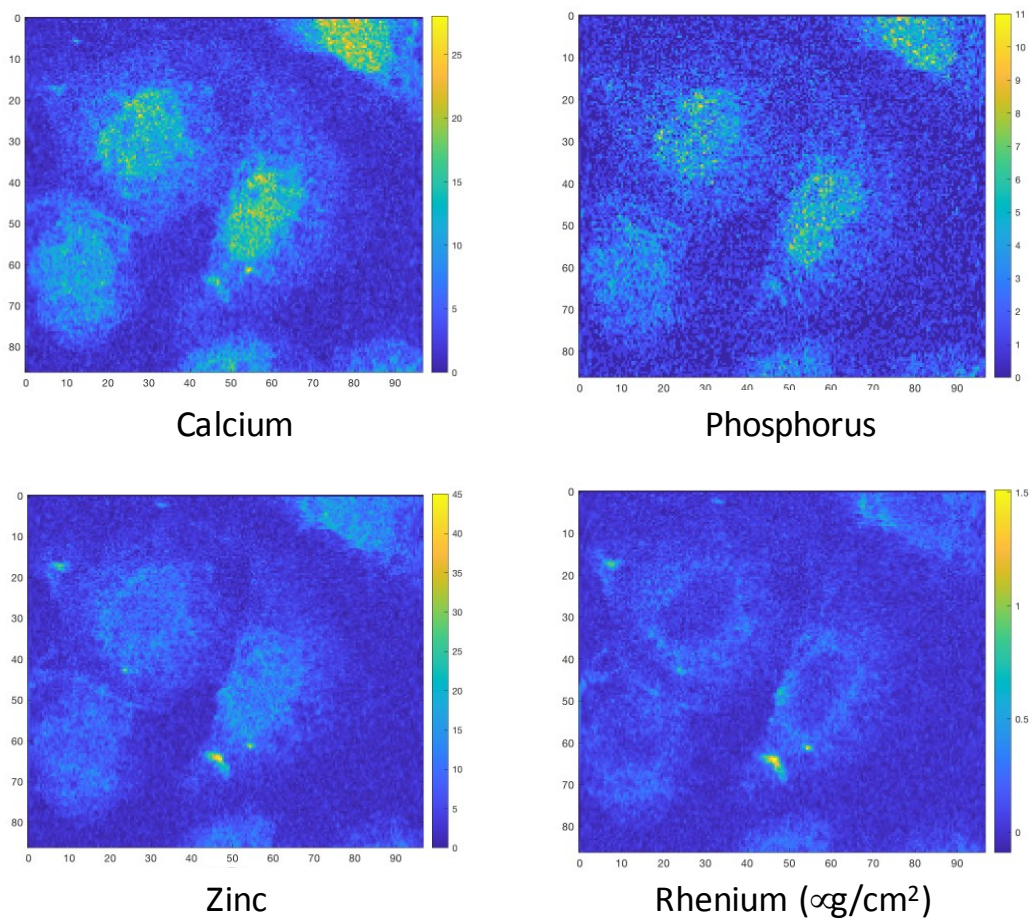
Figure S23. Elemental distributions of Ca, P, Re, and Zn in A549 cells incubated with **C3** (with color map (intensity) (right). The phosphorus (P), and zinc (Zn, Kβ-lines) maps are used to identify the nucleus area. Re was mapped using the Lß lines (~10.15 and 10.28 keV). A549 cells were incubated for 4 hours with **C3** (20 μM) before fixation and air-drying (excitation at 14 keV; integration time, 300 ms per pixel; pixel size, 500 nm). Scale axis in μm.
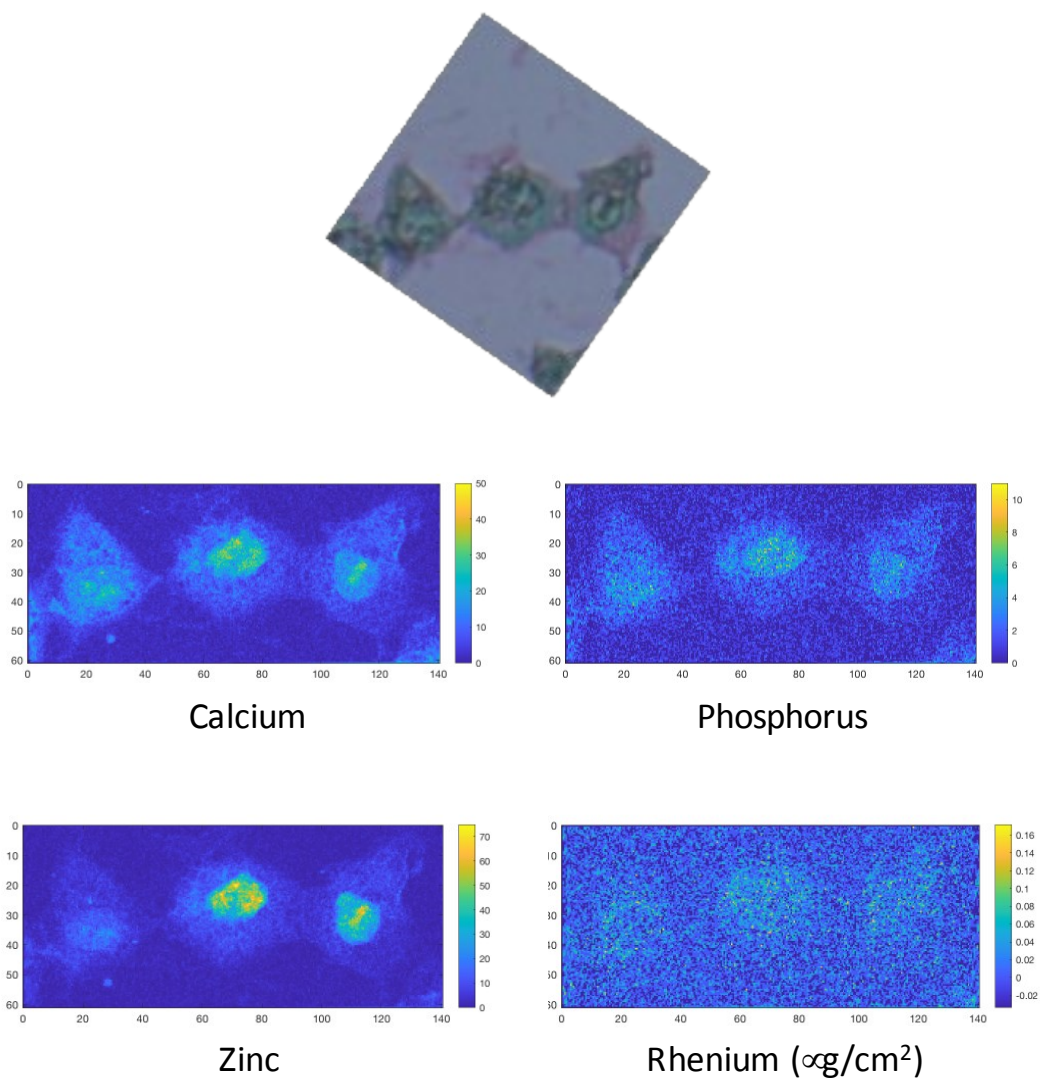
Figure S24. Elemental distributions of Ca, P, Re, and Zn in control A549 cells (with color map (intensity) (right) and corresponding transmission optical microscope image (top). The phosphorus (P), and zinc (Zn, Kβ-lines) maps are used to identify the nucleus area. Re was mapped using the Lβ lines (~10.15 and 10.28 keV). A549 cells were fixed and air-dried (excitation at 14 keV; integration time, 300 ms per pixel; pixel size, 500 nm). Scale axis in μm.
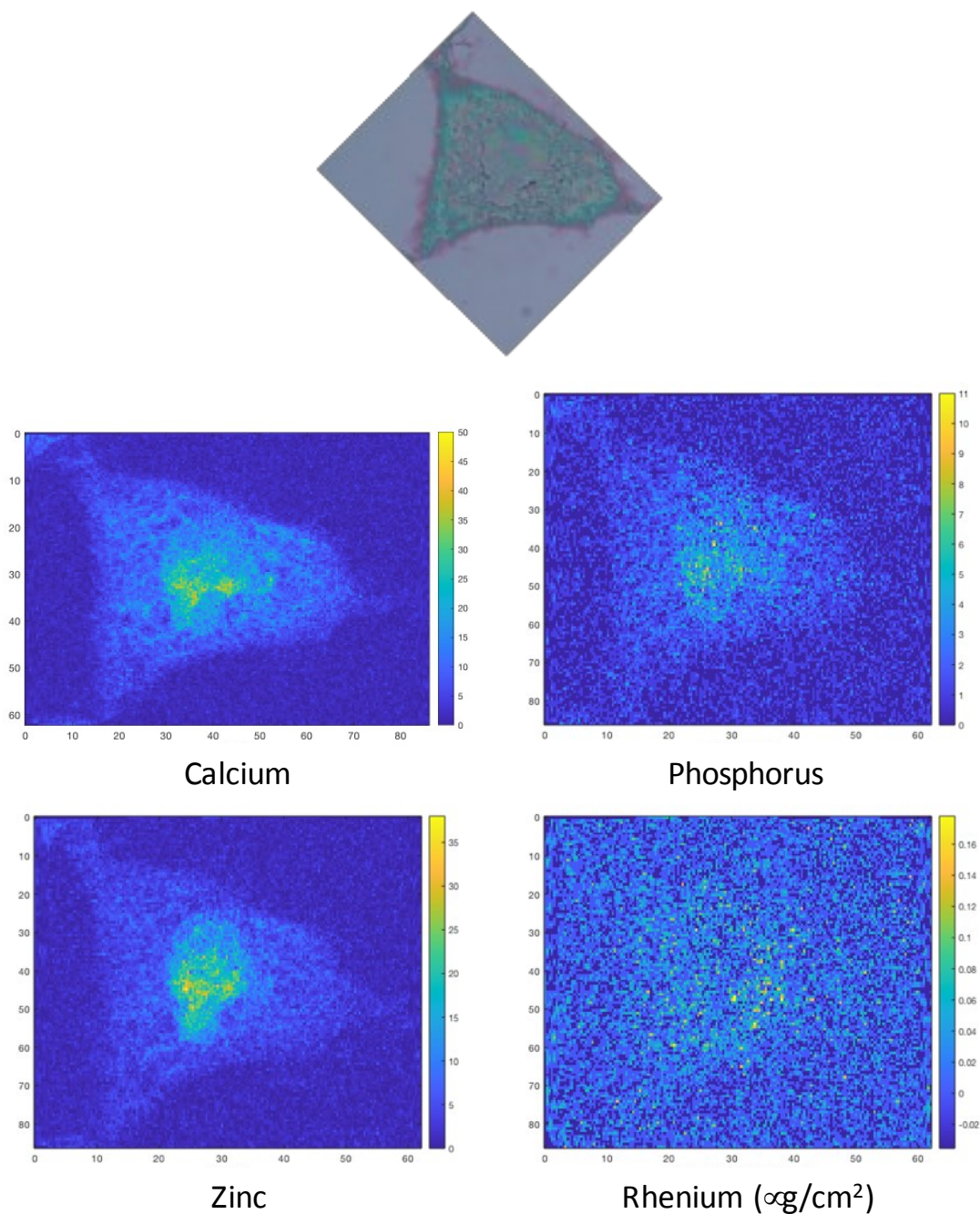
Figure S25. Elemental distributions of Ca, P, Re, and Zn in control A549 cells (with color map (intensity) (right) and corresponding transmission optical microscope image (top). The phosphorus (P), and zinc (Zn, Kβ-lines) maps are used to identify the nucleus area. Re was mapped using the Lß lines (~10.15 and 10.28 keV). A549 cells were fixed and air-dried (excitation at 14 keV; integration time, 300 ms per pixel; pixel size, 500 nm). Scale axis in μm.

Area 1

Calcium

Phosphorus

Zinc

Rhenium (∝g/cm²)

Area 2

Calcium

Phosphorus

Zinc

Rhenium (∝g/cm²)
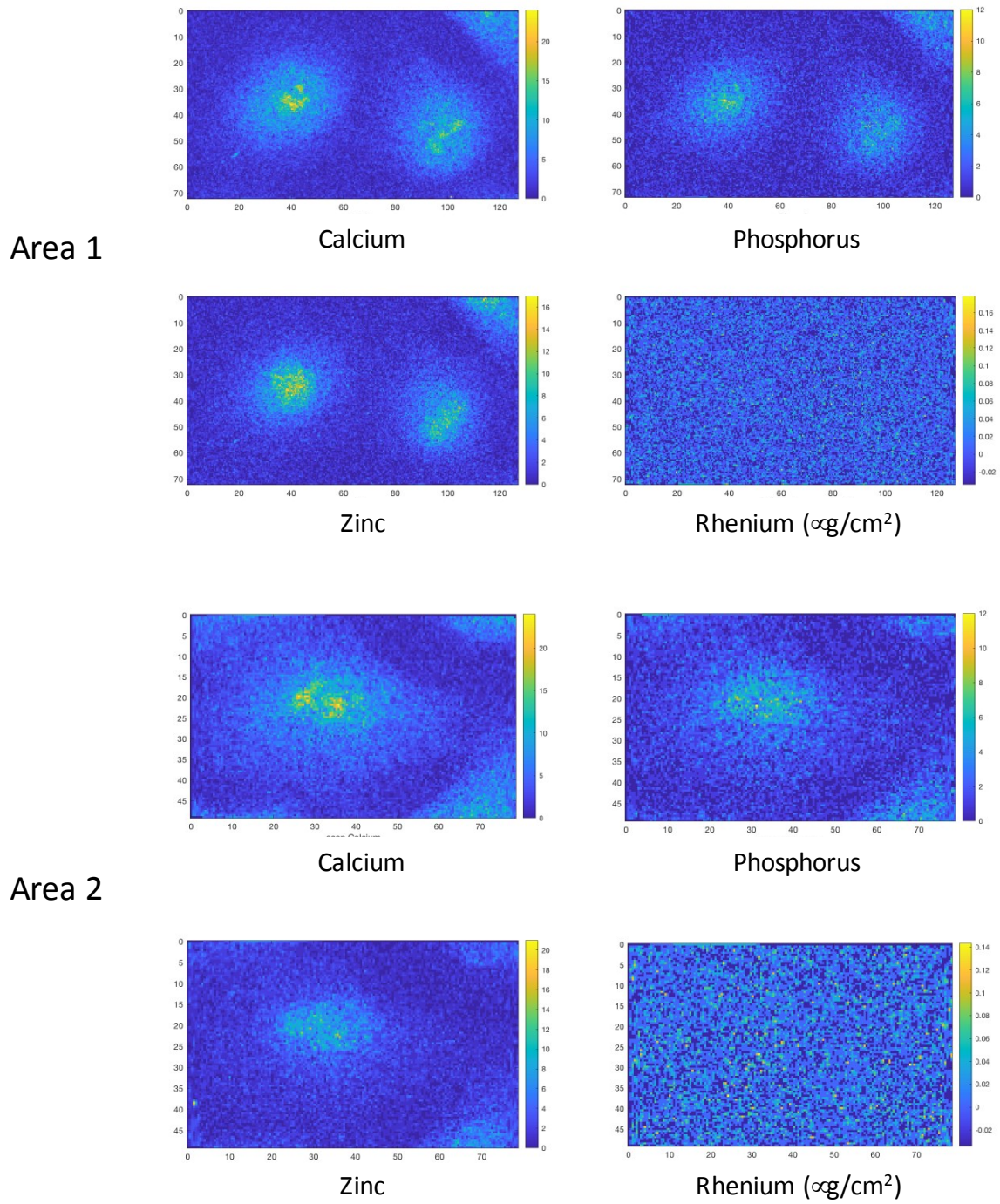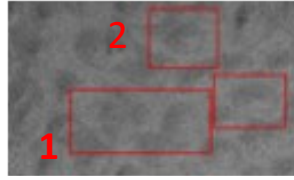
Figure S26. Elemental distributions of Ca, P, Re, and Zn in control A549 cells (with color map

(intensity) (right) and corresponding transmission optical microscope image (top). The phosphorus (P), and zinc (Zn, Kβ-lines) maps are used to identify the nucleus area. Re was mapped using the Lß lines (~10.15 and 10.28 keV). A549 cells were fixed and air-dried (excitation at 14 keV; integration time, 300 ms per pixel; pixel size, 500 nm). Scale axis in μm.
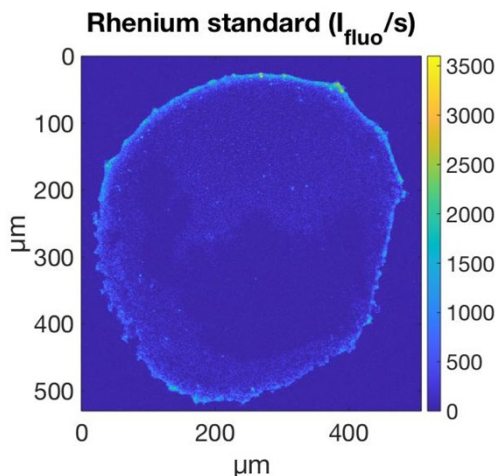
Figure S27. X-ray fluorescence imaging of a rhenium external standard (0.3 μL of a 10 μM rhenium solution) on a SiN$_3$ membrane (excitation at 14 keV; integration time, 10 ms per pixel; pixel size, 1 μm; I$_{fluo}$ = 2.32 x 10^7/s).

References

1. Maryanoff, B.E.; Reitz, A.B.; and Duhl-Emswiler, B.A., Stereochemistry of the Wittig reaction. Effect of nucleophilic groups in the phosphonium ylide, *J.Am.Chem.Soc.* **1985**, *107* (1), 217–226.

2. Bolte S., Cordelières F. P., A guided tour into subcellular colocalization analysis in light microscopy, *J. Microsc.,* **2006**, *224*, 213–232.

3. Hostachy, S.; Masuda, M.; Miki, T.; Hamachi, I.; Sagan, S.; Lequin, O.; Medjoubi, K.; Somogyi, A.; Delsuc, N.; Policar, C., Graftable SCoMPIs enable the labeling and X-ray fluorescence imaging of proteins. *Chem. Sci.* **2018,** *9* (19), 4483-4487.